A REANALYSIS OF THE ANOLE DEWLAP AT THE OSTEOLOGICAL, HISTOLOGICAL, AND MYOLOGICAL LEVELS

By

JACOB GEORGE

Bachelor of Science in Biology

West Virginia University

Morgantown, West Virginia

2020

Submitted to the Faculty of the
Graduate College of the
Oklahoma State University
in partial fulfillment of
the requirements for
the Degree of
MASTER OF SCIENCE
July, 2022

A REANALYSIS OF THE ANOLE DEWLAP
AT THE OSTEOLOGICAL, HISTOLOGICAL,
AND MYOLOGICAL LEVELS

Thesis Approved:

Dr. Haley O'Brien

Thesis Adviser

Dr. Holly Woodward Ballard

Dr. Paul Gignac

ACKNOWLEDGEMENTS

I would like to acknowledge Dr. Haley O'Brien, Dr. Paul Gignac, Dr. Holley Woodward Ballard, Dr. Ian Browne, Dr. Alex Claxton, Manon Wilson, Lyndon Wilson, and Holley Flora for their assistance, cooperation, and guidance throughout the completion of the research reported on in this thesis.

Name: JACOB GEORGE

Date of Degree: JULY, 2022

Title of Study: A REANALYSIS OF THE ANOLE DEWLAP AT THE OSTEOLOGICAL, HISTOLOGICAL, AND MYOLOGICAL LEVELS

Major Field: BIOMEDICAL SCIENCES

Abstract: A grounded understanding of the functional morphology of anatomical structures is essential to interpreting the observed dynamics of an organism's ecology. Anoles (Dactyloidae; *Anolis*) comprise a diverse grouping of small, arboreal lizards, constituting hundreds of species. The ecological literature on Anoles is robust, particularly surrounding their dewlaps: an elastic tissue fold which can be protruded into by the hyoid bones, which is used in both inter-and intraspecific interactions. This robustness of understanding ecological implications of the structure, however, is not paired with a robust understanding of the functional morphology of the dewlap, with centuries worth of analysis yet to yield a uniform conclusion. The goal of this study was to use modern digital and microanatomical methods to refine conclusions on the form and function of the anole dewlap. Firstly, I used diceCT (diffusible iodine-based contrast-enhanced computed tomography) protocols, paired with digital dissection in Avizo Lite 2021 to observe the small and delicate musculature attaching to the hyoid apparatus of *Anolis carolinensis* in both extended and relaxed positions to gain insight into the mechanism of action of dewlap extension. This analysis, while negating certain muscles from consideration of the extension mechanism, also implicated previously absolved muscles, while also revealing a potential new model of dewlap action. Secondly, I analyzed the anole hyoid apparatus histologically, including the application of Toluidine Blue staining protocols. These results, while solidifying the conclusions of previous research regarding the cartilaginous composition of the anole hyoid apparatus, also provided novel observations of fibrocartilage in the anole hyoid apparatus, as well as a potentially novel observed interaction between muscle and cartilage. A potential limitation of these analyses is the small sample size (n=8). Overall, these results provide the groundwork for expanded analysis of anole dewlap form and function, as well as the usage of *Anolis* as a model system for research on functional implications of unique structures in for the morphology, performance, fitness paradigm in extant and deep time contexts.

TABLE OF CONTENTS

Chapter Page

Chapter Page

LIST OF TABLES

Table Page

LIST OF FIGURES

Figure Page

CHAPTER I

AN INTRODUCTION TO MORPHOLOGY-PERFORMANCE-FITNESS, THE PHARYNGEAL ARCHES, AND ANOLES

Introduction

The impact of morphology on performance, and further the reciprocal effect of performance on fitness, is both an important and difficult to observe dynamic in biology (Arnold, 1983). Morphology encompasses the phenotypic characters of an organism, making it an important, initial driver of adaptation due to the variation of phenotypes within populations. This variation in morphological traits leads to differential physiological and biomechanical performance for different members of the population (e.g., capacity for expansion of the gular pouch in pelicans [Field et al, 2011], force exerted upon contraction of the pterygoids in crocodiles [Erickson et al, 2012], and speed of contraction of the plantaris muscle in kangaroo rats [Biwener et al, 1981]). Differential performance, in turn, impacts the fitness of said individuals within the population. Research models of morphology, performance, and fitness can therefore inform macroevolutionary processes, with or without a fossil record (e.g., reflecting whether deep-time phenotypes have been documented), especially when significant information about ecology is available. One such model is found in *Anolis* lizards (Squamata: genus *Anolis*): small lizards with a diverse array of ecologies, as well as unique intra- and inter-specific behaviors associated with their distinctive, generally bright colored dewlaps

(Nicholson et al, 2007). The anole dewlap is composed of an elastic integumentary tissue fold of the throat that is extended by the protrusion of the hyoid bones into the fold (Nicholson et al, 2007).

Understanding the morphology, performance, fitness dynamic can be contextualized through a multitude of factors, one of which is ontogeny. Ontogeny constitutes the development of an organism, from embryo to adulthood. During ontogeny, many organisms undergo significant morphological shifts, to the extent that some taxa may have completely different lifestyles as juveniles as opposed to adults (e.g., diets, ecologies; Gignac and O'Brien, 2016), and/or manifest sexual dimorphism, with the different activation and deactivation of genes leading to variable adult morphologies between the sexes (Williams and Carroll, 2009). Anoles are among the extensive list of taxa that display both notable shifts in ontogeny and distinct sexual dimorphism (Vanhooydonck et al, 2005), including development-specific changes in the phenotype of their dewlaps (Lailvaux et al, 2012), making them an excellent model for developmental studies.

Many important, observable ontogenetic shifts happen before parturition/hatching. During the embryological period, structures may develop that are later modified or even obliterated in the adult condition. Noteworthy structures of this category are the pharyngeal arches (Graham and Richardson, 2012), a set of serial homologues associated with the vertebrate head and neck comprised of mesoderm pouches (Figure 1.1). Each pharyngeal arch is composed of a nerve, cartilage, and arterial component. Constituents of the arches are differentially modified and obliterated across early embryonic development with the derivatives that persist forming specialized

structures in many vertebrates, including the hard (i.e., hyoid bones) and soft tissues (i.e., musculature) associated with the anole dewlap.

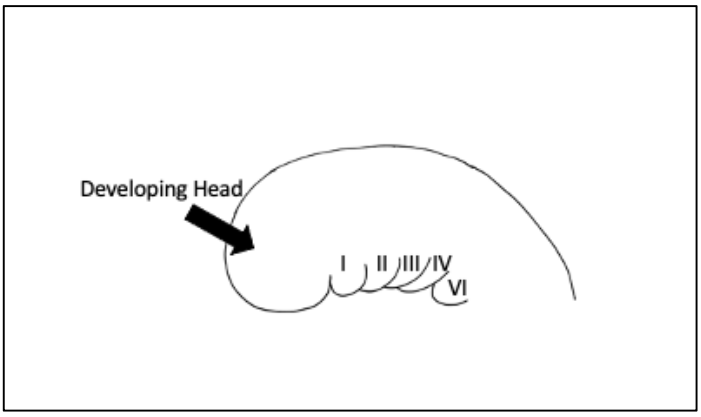

Figure 1.1. *Pharyngeal arches.* Simplified schematic of the pharyngeal arches displaying their relationship to each other and the developing head in tetrapods, such as Anoles. In tetrapods, arches I, II, III, IV, VI fully develop, with derivatives of each being represented in the adult morphology. Arch V does not fully develop, with its tissues quickly fusing with those of Arch IV. Image attribution: J. George.

Specific Aims

The specific aims of my thesis are threefold. First, I will address conflicts between conclusions on the form and function of the anole dewlap. This structure is important due to its use in intra- and interspecific interactions, with its variability in size, coloration, and sexual dimorphism (Nicholson et al, 2007; Vanhooydonck et al, 2005), making it an excellent target for analyzing the dynamic between morphology, performance, and fitness. Analyses have tended to focus on the jaws when targeting the morphology, performance, fitness model (e.g., Arnold, 1983). However, the jaws perform multiple functions, so while the morphology is consistent, interpreting the selective pressures influencing arch I may be a challenge (e.g., feeding [Neenan et al, 2014], respiration [Nunn et al, 1959], display [Williams, 2001]). As a whole, the dewlap has a specific function, greatly diminishing the many-to-one mapping conflicts when using it as a model for trait performance and evolution. With their developmental origins from the

pharyngeal arches, developmental limitations and innovations that impact the jaws also impact structures such as the dewlap. Second, while many researchers have attempted to understand the form and function of the anole dewlap (Bell, 1826; Von Geldern, 1919; Bels, 1990; Font and Rome, 1990), I aim to understand its structure in the context of modern anatomical visualization methods. Since the most recent, in-depth analyses of the form and function of the anole dewlap (Bels, 1990; Font and Rome, 1990), many new anatomical methods have come to prominence. Among these are diffusible iodine-based contrast-enhanced computed tomography (diceCT; Gignac et al, 2016) and digital dissection (reviewed by Lautenschlauger et al, 2014)). These methods are particularly helpful in observing the anatomy of small specimens, as well as delicate and intricate morphologies that cannot be observed using a destructive process, both of which apply to the anole dewlap. Third, I aim to understand the anole hyoid apparatus histologically, including aspects of its ontogeny and soft-tissue attachments. The microanatomy of the Anole hyoid remains relatively undescribed, due in part to its small and delicate nature, and the understanding of the origins and insertions of muscles and tendons, as well as the cartilage-to-bone transitions of the hyoid apparatus are important to fully mapping out how the structure operates biomechanically. By addressing aspects of the dewlap form within the context of competing functional hypotheses alongside its microanatomy, I aim to expand the potential for analysis of the anole dewlap and similar structures in deep time evolutionary contexts.

In the Beginning: Pharyngeal Arch Origins and Development

To understand development, form, and selective pressures on the Anole dewlap, as well as its relationship with the evolution of the craniocervical system, it is important

to understand the origins and development of the pharyngeal arches. The pharyngeal arches are a synapomorphy of Vertebrata (Graham and Richardson, 2012), but the developmental patterning of these structures lies deeper in the Deuterostomata, the bilaterian superphylum including taxa whose initial blastopore becomes the anus (Holland, 2002). In most deuterostomes, this developmental pathway presents as a set of structures referred to as pharyngeal slits (Graham and Richardson, 2012). These structures tend to be obliterated embryologically in echinoderms (Figure 1.2), leaving no discernible derivatives, but were present in basal echinoderms (Shu et al, 2002). Pharyngeal slits are present in the post-natal morphology of Hemichordata (Tassia et al, 2016), Tunicata (Schubert et al, 2006), and Cephalochordata (e.g., lancelets) (Figure 1.2). In lancelets, a multitude of pharyngeal slits develop, all serial homologues that are identical morphologically and functionally. While the pharyngeal slits are used in food collection in lancelets (Miyashita et al, 2021), it is difficult to discern whether this is the ancestral use of these structures, due to the derived position of lancelets (Schubert et al, 2006). In Vertebrata, this developmental pathway is most apparent in the embryo, but has been modified into diverse morphological structures in adults (Graham and Richardson, 2012).

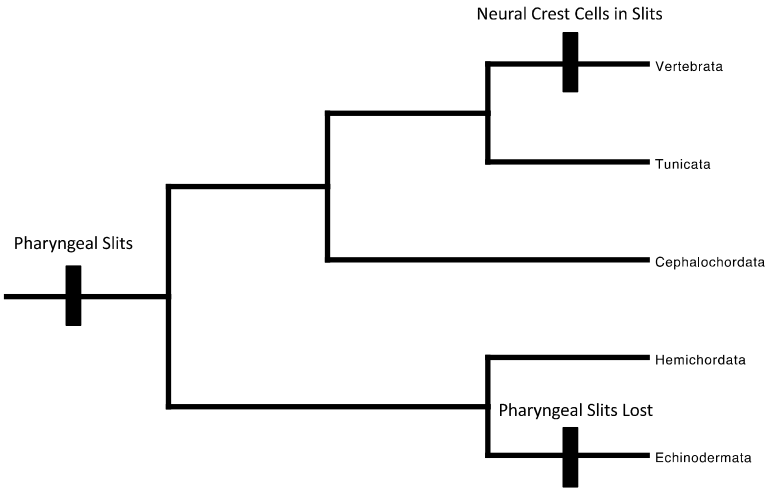

Figure 1.2. *Key events in pharyngeal slit evolution.* Phylogenetic tree of Deuterostomata highlighting significant events in the evolution of the pharyngeal slits. The pharyngeal slits are a derived character of Deuterostomata, with major transitions occurring in the Echinodermata and the Vertebrata. In Echinodermata, the pharyngeal slits are obliterated in early development. In Vertebrata, neural crest cells migrate into the pharyngeal slits, leading to a novel structure: the pharyngeal arches. Tree built using Mesquite.

In Vertebrata, this shift in pharyngeal slit development is attributable to a derived characteristic of the clade: neural crest cells (Hall, 2008). Neural crest cells are multipotent, embryonic cells that develop at the interface between the neural plate and the ectoderm (Hall, 2008), due to the combined activity of sonic hedgehog from the notochord, and BMP-4 and -7 from the ectoderm promoting the activity of chordin, noggin, and follistatin (Crane and Trainor, 2006). In ancestral vertebrates (Figure 1.2), these neural crest cells began to migrate into the pharyngeal slits during early development, leading to the derived status of these structures in vertebrates: the pharyngeal arches. The pathway of this migration is well understood, with migration occurring around the paraxial mesoderm into each respective arch. This redistribution of the neural crest cells preceded the development of novel, bony, innervated tissues from

these the pharyngeal slits, an adaption leading to many subsequent derived characters of the vertebrate cranial and cervical regions (Graham and Richardson, 2012).

The pharyngeal arches are a series of swellings that occur embryologically in the developing pharynx (regions that develop to constitute oral and cervical structures; Graham and Richardson, 2012). Many groups of deuterostomes develop dozens of pharyngeal slits; however, vertebrates have a reduced and variable number of pharyngeal arches (Graham and Richardson, 2012). Extant fishes, including cyclostomes (lampreys and hagfishes), develop seven arches or more, indicating that numerous arches is the ancestral condition for vertebrates (Shimeld, 2012). Amniotes (tetrapods that reproduce via the amniotic egg, including squamates, archosaurs, and mammals; Reisz, 1997) develop a total of five arches (Graham and Richardson, 2012). These are arches I, II, III, IV, and VI. In amniotes, arches IV and V fuse during early ontogeny (Figure 1.1). Each arch is comprised of a nerve, cartilage, and arterial component, contained within each swelling.

In ancient, basal fishes, the primary, externally observable arch derivatives were the gills, supported by a bony gill basket (Xian-guang, 2002). This feature is conserved in extant fishes (Graham and Richardson, 2012). This gill basket provides a rigid support system for the soft tissue structures responsible for respiratory gas exchange (Evans et al, 2005). For the first nearly one hundred million years of the evolutionary history of the lineage, few anatomical changes are known to have occurred in the bony gill basket of fishes (Graham and Richardson, 2012). In the Silurian (443–417 million years ago), the bony derivatives of the first arch began to exhibit flexures, bending forward during development, resulting in a mobile hinge protruding into the mouth: jaws. The long-term

implication of this modification was increased precision and directionality in the pursuit of food (Motta et al, 1991; Olivier et al, 2021; Rowe and Snively, 2022).

Jaws

These shifts in Arch I derivative morphology were driven by at least two crucial genes: *Dlx* and *Shh.* Mutations relating to these genes have precipitated the transition from jawlessness to jaws, as indicated by studies in the Cyclostomata (e.g., lampreys). In cyclostomes, *Dlx* is active in the first arch, allowing for rigid support of the mouth. However, in lampreys this structure cannot bend or flex (Kusakabe et al, 2007). In jawed vertebrates, *Shh* is also active in Arch I, indicating *Dlx* and *Shh* act in concert to produce the hinged vertebrate jaw (Graham and Richardson; Figure 1.3).

For millions of years, other clades of animals had structures that functioned to break down food resources that were too large to fit in their mouths, such as the chitinous beak of cephalopods (Klug et al, 2016) the modified anterior-most limbs of mandibulate arthropods (Rogers, 2002), and the chelicerae (claws) of chelicerate arthropods (Bicknell, 2018). Not unexpectedly, these animals tended to be the most prevalent predators in the ancient ecosystems of the Ordovician (485–444 million years ago) and Silurian, while also reaching sizes unfathomable for most other animals of the time (Klug et al, 2014). With the appearance of the vertebrate jaw, a diverse array of new ecospace became available to fishes, with some forms even displacing the cephalopods and arthropods as the predominant large predators in marine ecosystems (Dahl et al, 2010).

Novel Ecospace

Following the appearance of jaws, gnathostomes (jawed vertebrates) diversified rapidly into two major extant groups: the Chondrichthyans (cartilaginous fishes like

sharks and rays) and Osteichthyans (bony fishes like bass, catfish, swordfish) (Dearden, 2019). Jaws, paired with an increase in maximum size, led to gnathostomes invading newly exploitable niche space, with different taxa specializing into diverse feeding ecologies (Signor and Brett, 1984; Tapanila et al, 2013; Anderson and Westneat, 2007). Members of the Osteichthyan clade Sarcopterygii even invaded terrestrial ecosystems in the Devonian (419-359 million years ago), a lineage out of which the first tetrapods were derived (Ahlberg, 2019). The vertebrate jaw was critical in this sea-to-land transition, as the ability to precisely grab food proved essential in terrestrial ecosystems where food was no longer suspended in a water column. Over time, the structure and mechanism of action of the tetrapod jaw adapted to this lower density fluid, typified by a trend of decreasing bite force, and increasing bite efficiency (relative to *Acanthostega;* Neenan, 2014). These modifications led to a rapid diversification of tetrapods, with feeding ecologies including but not limited to hypercarnivores (Van Valkenburgh, 2007), megaherbivores (Fiorelli et al, 2013), generalists (Green, 2020), and scavengers (Ruxton and Houston, 2004).

Repurposing the Remaining Arches

During the vertebrate sea-to-land transition, many important modifications also occurred in the developmental pathways of the successive arches, serial homologues of Arch I (serially arranged structures derived from the same, segmental developmental pathways). In fishes this outcome is the gill arches. In osteichthyan fishes, arch II forms a major, distinctive, external structure: the operculum (Graham and Richardson, 2012) (Figure 1.3). Unlike chondrichthyans and cyclostomes, with gills covered by soft tissues, the osteichthyan operculum forms a protective hard tissue cover that opens on the

posterior aspect to sustain efficient flow of water over the gills. In amniotes the operculum develops in the embryo, but the posterior end completely seals, overgrowing the remaining arches and fusing with the ectoderm posteriorly (Graham and Richardson, 2012). In part, this change is connected to an adaptation of tetrapods: the lungs. In air-breathing tetrapods, these expandable and collapsible, sac-like, highly vascularized structures became the primary interface for respiration. With the gills and their related pharyngeal arch derivatives no longer being the primary interface of gas exchange, branchial openings to the external environment became deleterious (Lenfant and Johansen, 1972). For example, the improper closure of the opercular flap can lead to a malformed Cervical Sinus of His, the complications from which can require medical intervention (Adams et al, 2016). With this change, the posterior arch derivatives were freed to take on novel morphologies and functions. The bony derivatives of Arch II, for example, form most of the hyoid bones, which support the tongue (Auvenshine and Pettit, 2018). Thus, like the jaws, the derivatives of Arch II are of critical importance to food acquisition for amniotes.

The remaining bony derivatives of the arches III, IV, VI are greatly reduced, only developing into some laryngeal cartilages, such as the epiglottis, cricoid, and arytenoid cartilage (Maue and Dickson, 1971). These arches do, however, pattern vascular and nervous components that form important vessels in the cervical region and in association with the heart itself, as well as major cranial nerves (Graham and Richardson, 2016).

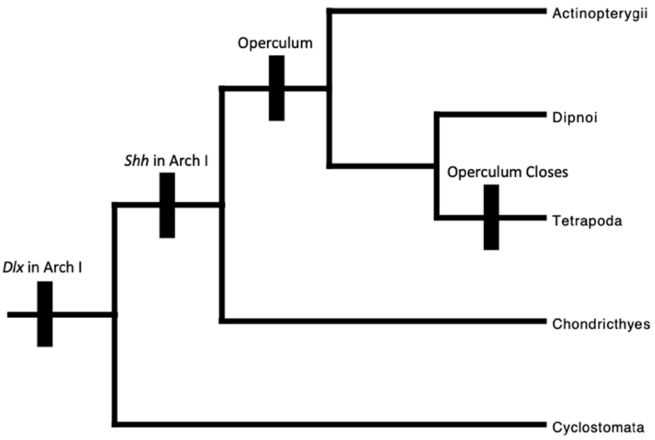

Figure 1.3. *Key events in pharyngeal arch evolution.* Phylogenetic tree of Vertebrata with major pharyngeal arch derivative transitions. The *Dlx* gene is active in many vertebrate clades, allowing for rigid support of the oral orifice. In gnathostomes, *Shh* gene activity in the first Arch allowed led to the evolution of the hinged vertebrate jaw. In Osteichthyans, a novel structure, the operculum, to cover the gill arches. In tetrapods, the developing operculum seals posteriorly, closing off the pharynx from the external environment. Tree built using Mesquite.

Primary Soft Tissue Derivatives of the Pharyngeal Arches

Each pharyngeal arch begins with the development of a cartilaginous core, while also being composed of a nervous and vascular component, all nested in the mesoderm of the arches (Graham and Richardson, 2012). Similar to the hard tissues patterned by the pharyngeal arches, the derivatives of their nervous, vascular, and muscular components also have direct functional significance.

Throughout evolutionary history, the nerve component of each arch has been substantially conserved, with each developing into a major cranial nerve (Table 1). The major cranial nerves include the trigeminal nerve (CN V) derived from Arch I, the facial nerve (CN VII) derived from arch II, the glossopharyngeal nerve (CN IX) derived from Arch III, and the superior and recurrent portions for the laryngeal nerve (CN X) derived from Arches IV and VI respectively (Kardong, 2009). Anatomical modifications to these

nerves generally follow modifications to the musculature and other soft tissues they innervate. For example, in mammals, the muscles of facial expression are derived from arch II and have migrated anteriorly to the cranial region, pulling the facial nerve with them (Burrows et al, 2006).

The vasculature derived from the pharyngeal arches is diverse in the adult morphology of vertebrates due to differential growth and obliteration. Evolutionarily, all these structures trace their origins to a tubular heart with bilaterally symmetrical vasculature that functioned as a single loop system (Stephenson et al, 2017). In, tetrapods a two-loop circulatory system (Stephenson et al, 2017) is thought to have evolved as a coordinated shift in cardiopulmonary morphology as gas exchange began to occur in the air-breathing lungs. This led to changes in the orientations and pathways of the major vessels around the heart, including the aortic arch and right subclavian artery (Arch IV), and the pulmonary artery (Arch VI; Kardong, 2009). Other major arteries derived from the pharyngeal arches in tetrapods (Table 1) include the maxillary and external carotid arteries (Arch I), the stapedial, hyoid, inferior tympanic, and ascending pharyngeal arteries (Arch II), and the common carotid arteries (Arch III; Kardong, 2009).

The muscular derivatives of the pharyngeal arches are also diverse in vertebrates, displaying an array of morphologies and functions (Table 1). These include adducting and depressing the jaw (masseter, temporalis, and pterygoids) (Hannam and McMillam, 1994), elevating and depressing the hyoid bones (stylohyoid, digastric, mylohyoid), and moving the tongue (stylohyoid and mylohyoid) (Hiiemae and Palmer, 2003). An exemplar evolutionary shift in the musculoskeletal configuration of the bony and muscular arch derivatives can be exemplified in mammals. Mammals have modified

portions of the jawbone (repeatedly) to form the mammalian middle ear (Maier and Ruf, 2016). These modifications have also led to significant morphological shifts in the musculature, with small muscles such as the stapedius (Borg and Zakrisson, 1975) and auricular (Yotsuyanagi, 2015) (both derived from arch II) used to stabilize and move the middle ear bones (Table 1). Another, less well-defined example of this is the dewlaps found in some squamates, such as the genus *Anolis*. In *Anolis*, the pharyngeal arch derived hyoid bones coordinate with the musculature and skin to form the extendable dewlap (Bels, 1990). However, unlike the well-defined function and evolutionary history of the mammalian middle ear, many aspects of the anole dewlap function and evolutionary history remain ambiguous.

Table 1.1. *Soft tissue pharyngeal arch derivatives.* Pharyngeal arch with nerve, vascular, and muscular derivatives. This table defines the structures as observed in amniotes, particularly Mammalia, where much study has been done due to their clinical significance. While the nervous and muscular derivatives are highly conserved, high variability can occur in the vascular derivatives. These structures are all associated with the cranial, cervical, or thorax regions.

Arch	Nerve Derivative	Arterial Derivative	Muscular Derivative
I	• Trigeminal Nerve (CN V)	• Maxillary • External Carotid • Artery of Pterygoid Canal	• Masseter • Temporalis • Pterygoids • Anterior Belly of Digastric • Mylohyoid • Tensor Tympani • Tensor Veli Palatini
II		• Ascending Pharyngeal • Inferior Tympanic	• Muscles of Facial Expression • Buccinator • Platysma • Stapedius

	• Facial Nerve (CN VII)	• Hyoid Artery • Stapedial Artery	• Stylohyoid • Posterior Belly of Digastric • Auricular
III	• Glossopharyngeal Nerve (CN IX)	• Common Carotid • Internal Carotid	• Stylopharyngeus
IV	• Vagus Nerve (CN X) • Superior Laryngeal Nerve	• Right: Subclavian • Left: Aortic Arch	• Cricothyroid • Intrinsic Muscles of Soft Palate
VI	• Vagus Nerve (CN X) • Recurrent Laryngeal Nerve	• Right: Pulmonary Artery • Left: Pulmonary Artery • Ductus Arteriosus	• Intrinsic Muscles of Larynx

Gular Pouches and Dewlaps

In some amniotes, the derivatives of Arch II have been the subject of numerous modifications via mutation and natural selection that have led to novel morphologies. They form distinctive, external structures that species use in food acquisition (the primary function of arch II derivatives: Field et al, 2011), or more exceptionally, for auditory (Geissman, 2000) and visual communication (Madsen et al, 2004). Arch II derived structures co-opted for communication tend to be grouped into two anatomical categories: gular pouches and dewlaps – protrusible and/or inflatable external soft tissues

supported by the hyoid skeleton. In extant taxa, gular pouches and dewlaps are present across many amniote groups. The abundance through deep time of these features is harder to discern as their soft tissues rarely fossilize (Briggs et al, 1997), and their hard tissues (the hyoid bones) inconsistently preserve (Li et al, 2018). When features are not abundantly present in the fossil record, phylogenetic comparative methods can be used to infer their evolutionary histories (Uyeda et al, 2018). While these methods remain unapplied for understanding the evolution of Arch II derived protrusible/inflatable structures across Tetrapoda, the current diversity of species that possess them implies that the developmental pathways and mechanisms for such structures is present in all amniote groups. This means they likely have had major morphological, functional, and ecological significance through time (Figure 1.4).

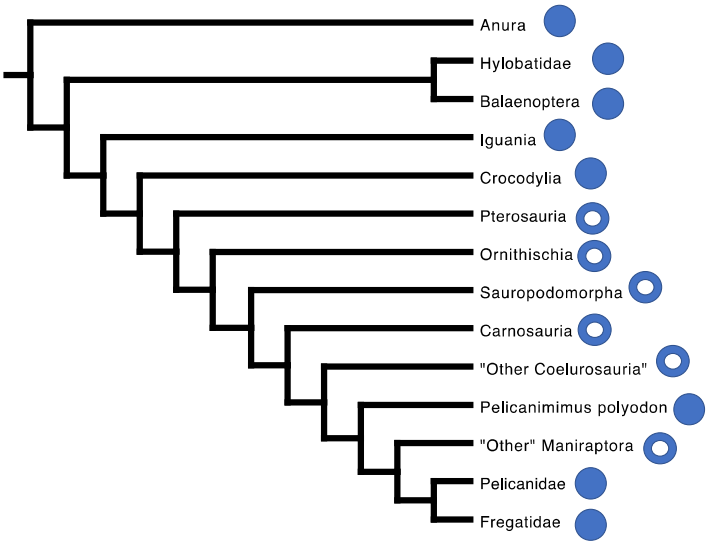

Figure 1.4. *Expandable gular structures in vertebrata.* Phylogenetic tree representing the distribution of expandable, pharyngeal derived structures in tetrapods. Representatives of all major tetrapod groups (Amphibia, Mammalia, Squamata, and Archosauria). Specific emphasis is placed on the Archosauria due to the presence of an apparent gular pouch structure in a fossil of the theropod *Pelicanimimus polyodon.* Closed circles indicate presence, open circles indicate absence or inconclusive. The prevalence across vertebrata

indicates that developmental pathways to form these structures were likely present in ancestral tetrapods. Tree built using Mesquite.

For the purposes of my research, the definitions of gular pouches and dewlaps are as follows, where both features consist of the skin that extends from the malar region to that of the thoracic inlet on the ventral surface of the neck, as well as their bony support structures:

1. Gular pouches are elastic tissue sacs, which are distinguished by the absence of bones that protrude into the negative space created during expansion. Gular pouches have a variety of functions, being used for as disparate of tasks as increased food intake, visual display, and auditory pitch modulation. Gular pouches are observed in Anurans (frogs) (Elias-Costas et al, 2017), Iguania (multiple species of chameleons), Crocodylia (crocodiles, alligators, gharials), Pelicanidae (pelicans), Fregatidae (Frigatebirds), Hylobatidae (siamangs), and Balaenoptera (rorqual baleen whales).
2. Dewlaps are distinguished by the presence of bones protruding into the negative space during expansion. As opposed to the gular "pouch", the elastic tissue of the dewlap is more akin to a fold, which the protruding bones (often the hyoid bones) push into to open the dewlap. Functionally, dewlaps are primarily used in visual display. Dewlaps are present only in squamates, specifically in the Iguania (e.g., iguanas, anoles, and agamids), with many members of these taxa and their relatives convergently evolving dewlaps (Ord et al, 2015).

Genus Profile: *Anolis*

Anoles are a speciose family within the Iguania, Dactyloidae, comprising the over 400 species in the genus *Anolis* alone (Nicholson et al, 2007). Anoles have a geographic range extending from southern North America to central South America, as well as on multiple offshore islands, with particularly high diversity in the Caribbean Archipelago (Langerhans, 2007). Most anoles are small, with the largest species, *Anolis equestris*, measuring between 33-51 cm in total length. Many anole species are arboreal, succeeding in a variety of ecological ranges spanning from the ground to canopy level (Langerhans, 2007).

Anoles are characterized by their dewlaps, which are supported by their hyoid bones (Figure 1.5) (Figure 1.6). Most species of anoles have dewlaps, with those without dewlaps being nested within their phylogenetic tree. This indicates that the dewlap is an ancestral trait for the genus that has been secondarily lost in some species (Nicholson et al, 2007). The dewlap is important to anole ecology, used in both intra- and interspecific interactions. The dewlap is extended and retracted as part of a complex visual display, syncing up with a coordinated fore-limb pushup motion. This display is used for attracting mates and intimidating conspecific aggressors. The dewlaps themselves demonstrate a variety of colors, patterns, and shapes, with some species presenting notable sexual dimorphism (Nicholson et al, 2007). While much work has been done on the anole dewlap, a disproportionate amount of this work has focused on the ecological implications of the structure, as opposed to its form and function.

Figure 1.5. *Anole dewlap display.* Male Carolina Anole (*Anolis carolinensis*) with dewlap relaxed (top) and extended (bottom). During this interaction the male was displaying to a female. Photos taken by author in Hilton Head, South Carolina.

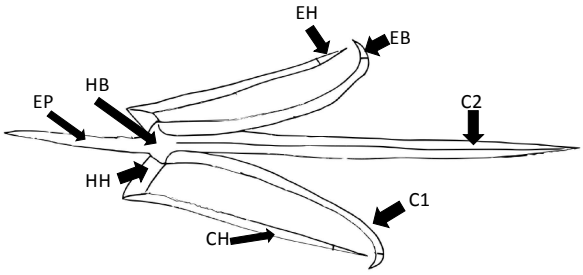

Figure 1.6. *Anole hyoid apparatus.* Simplified diagram of the hyoid bones of *Anolis*. Abbreviations: EP, entoglossal process; HB, hyoid body; HH, hypohyal; CH, ceratohyal; EH, epihyal; C1, first ceratobranchial; EB, epibranchial; C2, second ceratobranchial.

Anole Dewlap Form and Function

While less prevalent than ecological studies, work by functional morphologists has attempted to understand the form and function of the anole dewlap for centuries. Early work included that of T. Bell, who concluded in 1826 that the dewlap fold was supported by the hyoid bones (Bell, 1826). Over the next 160 years, researchers tried to

deduce what muscle were involved in the action of dewlap extension by analyzing the gross anatomy of the muscles associated with the hyoid apparatus (Figure 1.7). Proposed mechanisms included primary action of the *M. sternohyoideus* (Bell, 1826), the *M. ceratohyoideus* (Von Geldern, 1919), and even incorporating the movement of the tongue (Gnanamuthu, 1937). However, in 1990 two teams took different approaches, applying the most up-to-date experimental methods available at that time.

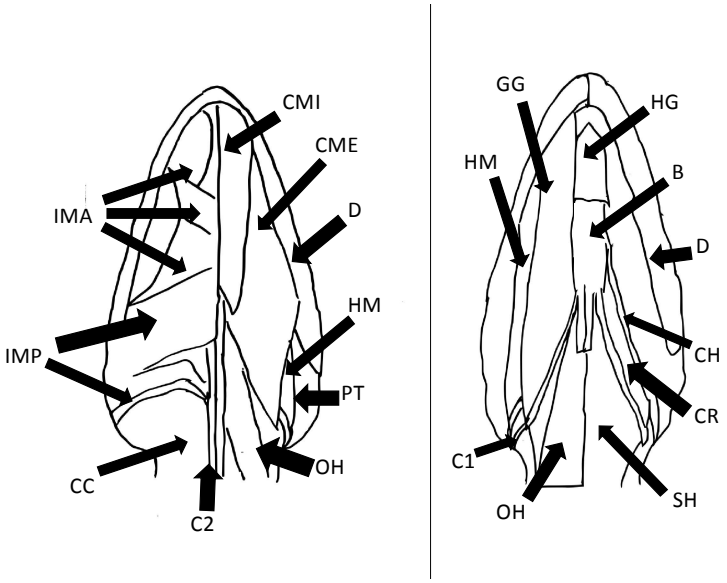

Figure 1.7. *Previous descriptions of anole hyoid musculature.* Simplified diagram of *Anolis* hyoid musculature from the ventral aspect, modified from Font and Rome, 1990. Left image portrays superficial hyoid musculature, while the right image portrays deep musculature. Abbreviations: B, hyoid body; CC, *M. constrictor colli*; CH, ceratohyal; CME, *M. ceratomandibularis externus*; CMI, *M. ceratomandibularis internus*; CR, *M. ceratohyoideus*; C1, first ceratobranchial; C2, second ceratobranchial; D, dentary; GG, *M. genioglossus*; HG. *M. hyoglossus*; HM. *M. hyomandibularis*; PT, *M. pterygoideus*; OH, *M. omohyoideus*; SH, *M. sternohyoideus*.

Vincent Bels employed electromyography and electrical stimulation of the hyoid musculature using *Anolis carolinensis* (Bels, 1990), and Enrique Font and Lawrence Rome employed cinefluoroscopy and high-speed cameras using *Anolis equestris* (Font and Rome, 1990), respectively, to observe the action of the anole dewlap apparatus. Both groups reached the same conclusion regarding the involvement of the second

ceratobranchial bones of the hyoid apparatus. During the opening of the dewlap, the paired second ceratobranchial bones swing forward, pushing out into the dewlap skin fold, thereby opening the dewlap for display. The groups, however, conflicted on the actions of the other parts of the hyoid apparatus and the associated musculature. Bels concluded that during the opening of the dewlap the hyoid apparatus moves anteriorly and depresses towards the tip of the jaw, with the action being driven primarily by the *M. branchiohyoideus* leading to a coordinated motion into the displacement of the second ceratobranchial. Font and Rome concluded that the hyoid apparatus is pulled posteriorly towards the torso, with the action being driven primarily by the *M. ceratohyoideus*, (a muscle that has been defined as equivalent to the *M. branchiohyoideus*: Edgeworth, 1935) leading to the displacement of the second ceratobranchial. These lead to mutually exclusive conclusions on the action of the hyoid bones and musculature, with conflicting implications for *the M. ceratohyoideus* in the opening of the anole dewlap (Figure 1.8).

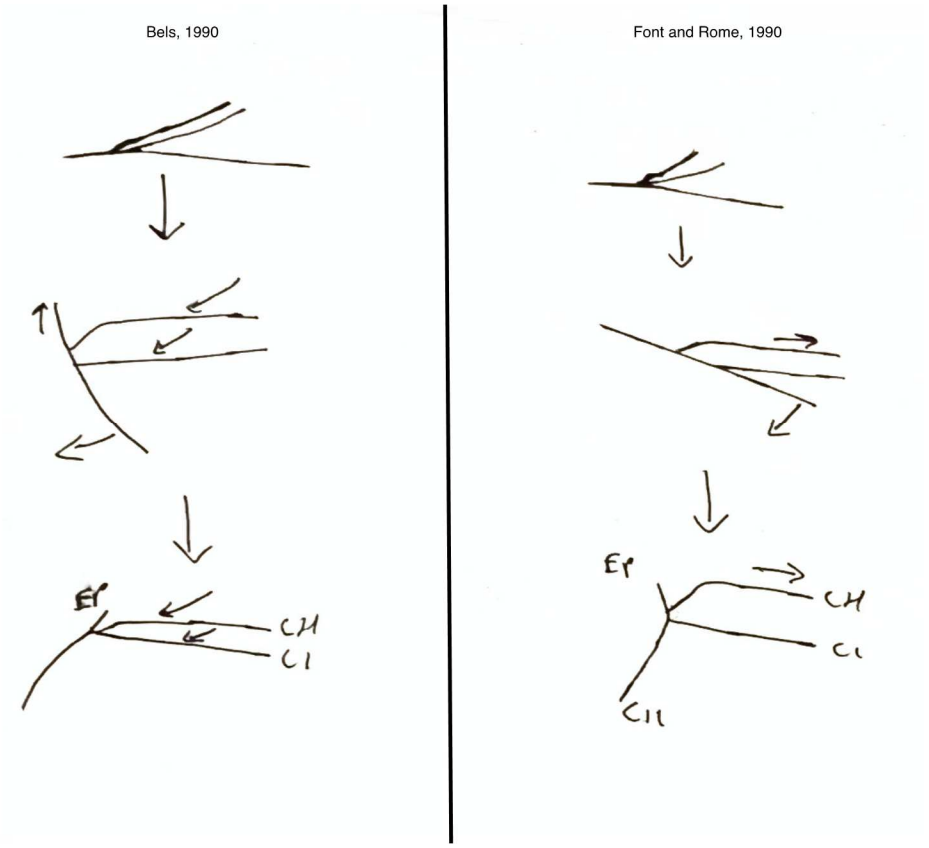

Figure 1.8. *Models of anole dewlap extension.* Comparison of mechanism of action of the anole dewlap based on Bels, 1990 (Left) and Font and Rome, 1990 (Right). In both models the second ceratobranchials protrude into the dewlap fold during extension. Note specifically each model's movement of the ceratohyals, for which the models conclude opposite directions of displacement relative to the relaxed position. The Bels model displaces the ceratohyals anteriorly, while the Font and Rome model displaces the ceratohyals posteriorly. Bones presented are Ceratohyals (CH), Entoglossal Process (EP), the First Ceratobranchials (CI), and the Second Ceratobranchials (CII).

Both studies also explored the histology of the hyoid apparatus, with similar observations recorded. Font and Rome (employing Milligan trichrome and alizarine red staining) found the first ceratobranchials to be the only ossified components of the hyoid apparatus, which were dorsoventrally flattened in cross section (Font and Rome, 1990). The remaining components were all found to be cartilaginous, with chondrocytes organized into groups of four. The second ceratobranchials specifically had calcium deposits organized in a semicircular pattern. Bels found similar results regarding

ossification (employing alizarine red and alcian blue staining), with only the first ceratobranchials being ossified. They found the chondrocytes however, to be arranged in groups of two or three. They also found the mineralization pattern of the second ceratobranchials to be in a semicircular pattern. Overall, these disparate functional hypotheses and morphological conclusions suggest a need for additional study, employing a more modern anatomical analysis, such as digital dissection.

Benefits of Digital Dissection

Recent technological innovation has provided a method of analysis that these previous studies did not have access to, digital dissection. Through modern imaging techniques, we are now able to pair 3D visualization programs with tomographic scan data (e.g., computed tomography [CT] and magnetic resonance imaging [MRI]) to analyze and trace (segment) structures *in silico*, allowing in-situ observation without risking damaging them using standard gross dissection protocols (Lautenschlager et al, 2014). This is of great importance when analyzing small, delicate, and intricate structures and/or specimens, which could be destroyed using traditional dissection methods (Cox and Faulkes, 2014).

Diffusible Iodine-Based Contrast-Enhanced Computed Tomography

While imaging technologies such as CT and microCT scanning have greatly enhanced our ability to image organismal morphology, these X-ray-based methods are ineffective for imaging soft tissues. To render soft tissues visible with X-rays, they must first be rendered radiopaque: specimens/tissues are often bathed in staining agents to increase contrast. A novel method for this staining is diffusible iodine-based contrast-enhanced computed tomography (diceCT) (Gignac et al, 2016). Using different iodine-

based compounds (I_2KI, I_2E, I_2M) as the staining agent, this method allows for effective and precise analysis of soft tissues, particularly in nervous (Gignac et al, 2016) and muscular structures (Gignac et al, 2016), due to the differential binding of the iodine to tissues based on their structural composition; for example: myelinated versus non-myelinated nervous structures, and to oxidative versus glycolytic fibers of muscles (Gignac et al, 2016).

Meeting Specific Aims

For this thesis, I address the above-outlined specific aims by revisiting the form and function of the anole dewlap using the most up to date and modernized methods at my disposal. The combination of diceCT and digital imaging has not previously been used to analyze the structure of the anole hyoid musculature in reference to its function, and the ability to analyze muscles by their morphology, down to the fascicular level, offers a new level of detail that previous research on this structure has been unable to achieve. To further understand the microanatomy of the hyoid bones, I employed histological methods and tissue staining with toluidine blue, a staining agent that previous studies did not apply. I also directly compared the hyoid bone histology of male and female specimens to search for indicators of the ontogenetic shifts that lead to the hypermorphed dewlap structure of the male anole, as compared to the female phenotype. Through these methods my goal was to build on previous work on the form and function of the anole dewlap, to resolve the conflicts present in the most recent research on the structure, and to build a framework to employ anoles as a model for studies within deep time evolutionary contexts.

CHAPTER II

DIGITAL DISSECTION OF THE ANOLE MUSCULOSKELETAL SYSTEM

Introduction

The musculoskeletal system is critical to the morphology, performance, fitness paradigm (Arnold, 1983), as it facilitates the biomechanical effort required for the body's structures to apply force. Many structures in the musculoskeletal system act as one of three different classes of levers by combining the rigid support of the skeleton (lever arm) and movement about a joint (fulcrum) with the extensile and contractile properties of the muscular system (effector; Westneat, 2004). Classic examples include the vertebrate jaw joint and the vertebrate elbow joint (third class levers; Koolstra and van Eijden, 2005; Fornalski et al, 2003) the talocrural joint (second class lever; Scott and Winter, 1991), and the atlanto-occipital joint (first class lever; Mandarim-de-Lacerda, 2019). Levers within the vertebrate Bauplan have evolved for mechanical, display, and other functions, with some taxa developing specialized systems via unique anatomical structures. One example of this is the dewlap system of *Anolis* lizards. In anoles, the hyoid apparatus has been modified into a first order lever, whereby muscular action on the hyoid elements causes the second ceratobranchials swing anteriorly and ventrally (Bels 1990; Font and Rome 1990), protruding a fold of often brightly colored skin for both intraspecific and interspecific display (Nicholson, 2007).

The analysis of musculature is as old as the study of anatomy itself. Gross anatomical

dissection to understand the form and function of musculature has been performed for centuries (if not millennia) in models such as humans (Brenna, 2022), sharks (Peabody, 1897), and even anoles (Bell, 1826). Gross anatomical dissection is a highly invasive practice, with many small and delicate muscles being destroyed during dissection (Lautenschlager, 2014). The inherent invasiveness of the practice also makes it particularly difficult to observe and describe the musculature of small taxa by gross dissection (Cox and Faulkes, 2014). This makes the detailed descriptions of the musculature by gross dissection of taxa such as anoles difficult, due to their combination of small size with intricate and delicate musculature (particularly in their craniocervical region).

The hyoid apparatus of tetrapods represents a derived condition of the fish gill basket, with delicate, homologous features identifiable between the two structures, including bones (Dearden et al, 2019). The overall composition of the hyoid apparatus is conserved across lepidosaurs: tuataras and squamates (Figure 2.1). It consists of a single, midline main hyoid body (basihyal) and entoglossal process, as well as bilaterally paired and elongate hypohyals, ceratohyals, epihyals, epibranchials, first ceratobranchials, and second ceratobranchials. The basihyal is the central component of the structure, from which the remaining elements articulate and project. The entoglossal process of the basihyal projects anteriorly from the hyoid body into the tongue. The hypohyals project anterolaterally from the lateral surface of the basihyal, and at their distal aspect form a joint with the ceratohyals, which project posterolaterally. At the tips of the ceratohyals are the epihyals, which project dorsally. Projecting posterolaterally from the lateral surface of the basihyal are the first ceratobranchials, which are tipped by the small

epibranchials. Lastly, the second ceratobranchials project posteriorly from the posterior surface of the hyoid body.

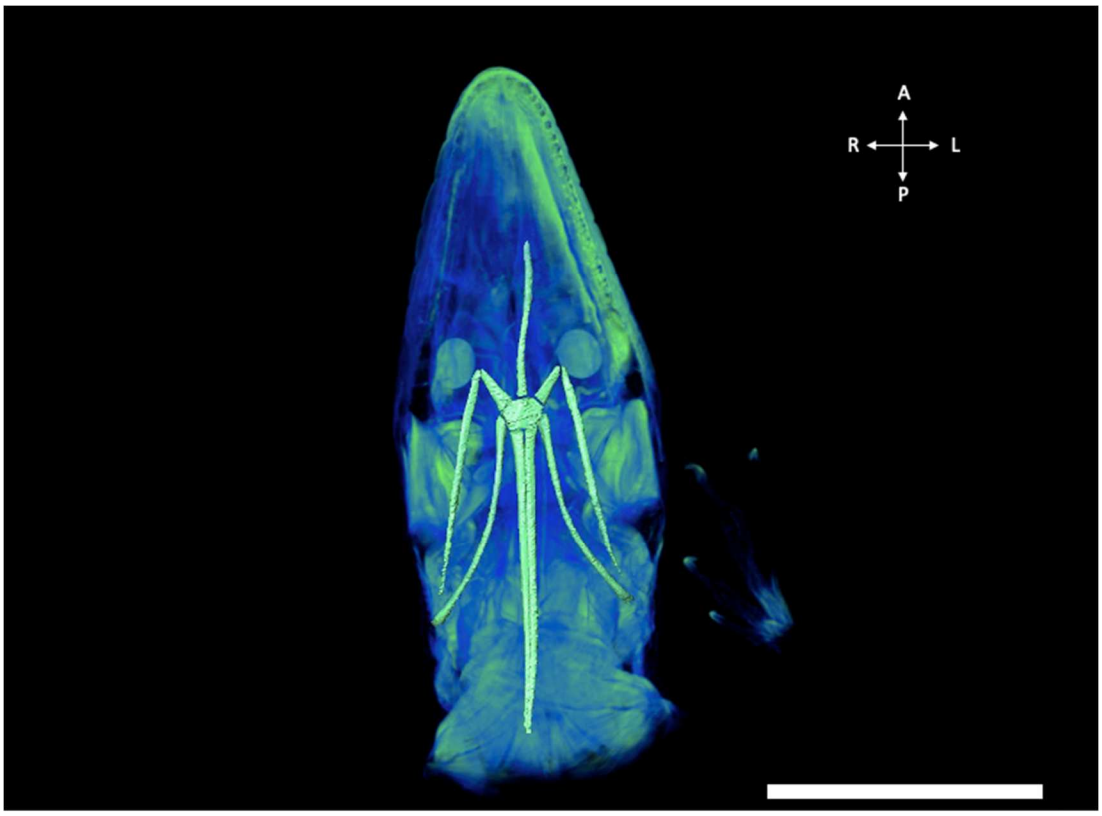

Figure 2.1. *Squamate hyoid apparatus*. Squamate hyoid apparatus (light green) represented in a semitransparent *Anolis carolinensis* specimen, displaying positioning in craniocervical region in ventral view. Scale bar = 5mm. Compass rose orientations: Anterior (A), Posterior (P), Left (L), Right (R).

The presence of many muscles associated with the hyoid apparatus is also conserved in lepidosaurs, such as the *Musculus hyoglossus*, *M. sternohyoideus*, and *M. omohyoideus*. From this conserved framework, extant squamates use this musculature to perform a variety of complex functions with the hyoid apparatus. These include projectile tongues in chameleons for food acquisition (Herrel et al, 2001), the ability to move air in and out of the lungs using gular pumping by monitor lizards (Owerkowicz et al, 1999), and in some members of Iguania, complex cervical display structures. The Iguania includes taxa bearing and often named after these display structures such as frilled-neck and fan-throated lizards, and dewlap-projecting anole lizards (Ord et al, 2015). These

structures are distinctive to Iguania, with the skeletal components projecting into the external flaps of cervical integument and associated hyoid musculature effecting their opening and closing in conjunction with display behaviors. Of these iguanian cervical display structures, the dewlap of the *Anolis* lizards is best studied.

The history of research on the action of the anole dewlap is complex, with at least four different proposed models implicating different muscles as the primary effector of ceratobranchial (and therefore dewlap) extension. Among the oldest models is that of T. Bell (1826), who implicated the *M. sternohyoideus* as the primary driver of dewlap extension by pulling the hyoid body posteriorly, causing the projection of the second ceratobranchials into the skin of the throat. Following this foundational work, a variety of models were proposed, including implications of the action of the *M. hyoglossus* pulling the hyoid body forward from its anterior aspect (Gnanamuthu, 1937; Bellairs, 1970), and the contraction of the *M. ceratohyoideus* pulling the hyoid body and displacing the second ceratobranchials anteroventrally (von Geldern, 1919). Jenssen (1978) implicated another muscle of interest: the *M. omohyoideus*, with its positioning between the scapula and hyoid apparatus making it an intriguing bridge between the dewlap action, and the pectoral-mediated "push-up" display behavior that is often associated with its extension (Jenssen, 1978). Most recently, analyses using electromyography on *Anolis equestris* (Font and Rome, 1990) and radiography on *Anolis carolinensis* (Bels, 1990) were employed to evaluate musculoskeletal actions more directly. While these studies conflict on the interpretation of structural action (Figure 1.8), both implicate the *M. ceratohyoideus* as the primary driver of dewlap extension. A contributing aspect to these conflicts in structural action may be the multiple magnitude size difference between *A.*

equestris and *A. carolinensis*, with the differential forces and output necessary leading to different mechanisms of action to achieve the same functional outcome. Size-related dewlap functional hypotheses remain un-investigated.

In recent decades, the observation of form and function of the musculoskeletal system has been revolutionized by methods of digital imaging and dissection. By using image capturing methods such as computed-tomography and magnetic resonance imaging, anatomical data sets can be digitally dissected with imaging software. Contrast-enhancement procedures prior to image acquisition enable additional, noninvasive analysis of soft tissues, such as muscles and nerves, even on small and delicate structures and/or specimens (Cox and Faulkes, 2014), such as the musculature of the anole hyoid apparatus.

Here, I digital dissected the hyoid musculature of *Anolis carolinensis* using these modern methods, with the specific aim of re-evaluating the conflicts between the conclusions of Bels (1990), Font and Rome (1990), and earlier models (Bell, 1826; Geldern, 1919: Gnanamathu, 1937), regarding the contribution of the *M. ceratohyoideus*, *M. hyoglossus*, *M. omohyoideus*, and *M. sternohyoideus* in the action of extending the anole dewlap. These previous analyses employed gross dissection, whereas I employ contrast-enhanced procedures, giving my analyses a less invasive approach with which to view the anole hyoid musculature *in situ*. Further, I aim to digitally dissect this musculature with the dewlap in relaxed and extended positions, to identify whether differences in muscle and bone positioning / interactions are visible, and whether these differences support or refute earlier hypotheses.

To meet this aim, I will employ diffusible iodine-based contrast-enhanced computed tomography (diceCT). DiceCT is a staining method that uses iodine-based compounds (iodine potassium iodide solution [I_2KI]; iodine in ethanol solution [I_2E]; iodine in methanol solution [I_2M]) to provide increased radiodensity of soft tissues for CT imaging, with the most used solution being Lugol's Iodine: I_2KI (Gignac and Kley, 2014; Gignac et al., 2016). Iodine differentially binds to soft tissues based on their structure and composition by preferentially binding to fats and carbohydrates allowing for effective, noninvasive analysis of soft tissues, such as nerves and musculature (Gignac et al, 2016), via increased X-ray densities. This makes it optimal for the analysis of small and delicate morphologies (Camilieri-Asch et al, 2020), such as the anole hyoid apparatus and associated musculature. Use of diceCT in the context of this study helps achieve my specific aims by parsing out distinctive characteristics of the hyoid musculature that were destructively sampled in previous studies. Maintaining the muscle associations is beneficial because it allows a more robust analysis of the relationships between the structures. Using 3D printed designs, I manipulate the hyoid musculature into an extended position to be able to analyze the muscles in this position *in situ* with digital dissection.

Methods: Digital Dissection

Specimens

For this study, nine specimens of *A. carolinensis* were digitally dissected. Eight of the specimens were obtained from Ward's Science (Rochester, New York), and were deceased when obtained. These specimens were fixed in formalin by Ward's Science, and their provenance is unknown. An additional specimen was donated by Dr. Eric McElroy.

This wild-caught specimen was captured in the Charleston, South Carolina area, and euthanized for an unrelated study, under an appropriate IACUC protocol approved by the College of Charleston. Because specimens were obtained as cadaveric materials, no IACUC protocol was required for this study.

Designing Brace Harnesses

In effort to reposition the hyoid musculature from its relaxed position to its extended position, novel, 3D printed brace harnesses were designed using Fusion 360 (V.2.0.10244, Autodesk, California) software. A digital, 3D model of one anole specimen was rendered in Avizo to use as a scale reference for designing the apparatus. Six design iterations were trialed. The final design comprised of bendable tabs, which allowed the harness to wrap around the torso of the specimen with small "teeth" included to assist in gripping the anole's skin (Figure 2.2). The harness included an insertion point, wherein a piece of 3D printer filament with a 1.75 mm diameter was placed. The devices were printed using a Prusa Mark 3s 3D printer (Prusa Research, Czech Republic).

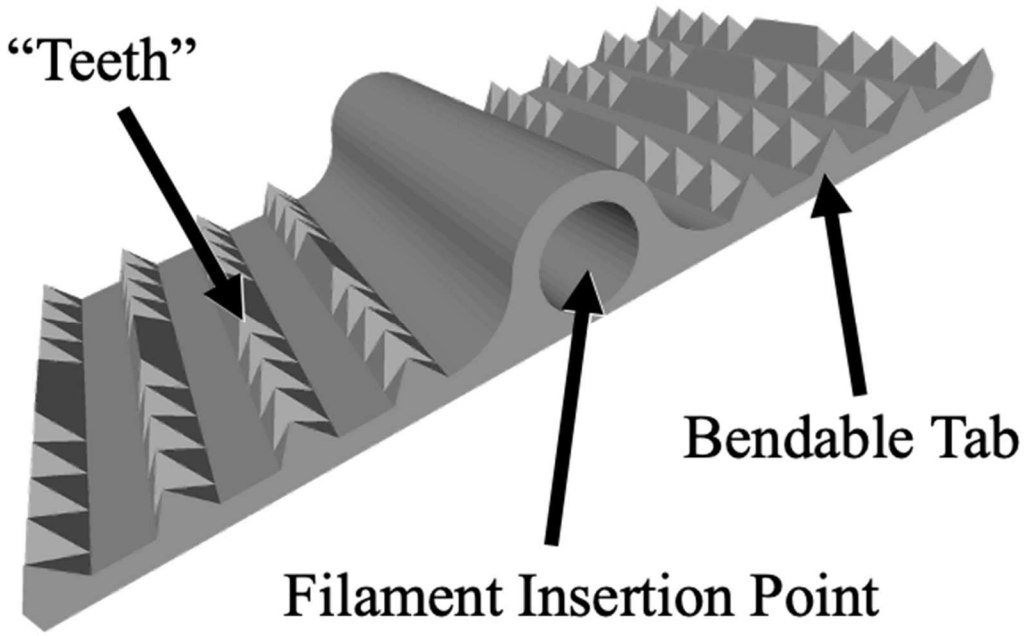

Figure 2.2. *Brace harness design.* 3D rendering of final brace harness design. Note the tabs, teeth, and insertion point for filament.

Rehydration of Specimens

To restore mobility to the stiff, formalin-fixed specimens, they were rehydrated (after Singer et al., 2014). This method calls for soaking of the specimens in deionized water in a sealed chamber to allow water to diffuse into the tissues and formalin to diffuse out. Antifungal agents are also placed in the chamber to prevent decomposition of the specimen. Our study used a two-container system: first, specimens were placed into a container filled with deionized water, adding Damprid crystals as the antifungal agent. This container was left unsealed, and was placed into a larger, second container that served as the sealed chamber. Extra Damprid crystals were scattered within the larger container. Specimens were re-hydrated for one month, with the deionized water changed out every 2–3 days to prevent stagnation. The rehydration of the specimens returned

some of the in-life malleability to the specimens, but not enough to restore full elasticity to the dewlap fold. During the rehydration process, specimen manipulation was attempted by using forceps in an effort to extend the hyoid bones with the dewlap fold as a replication of ecological studies on the genus (Nicholson et al, 2007). The specimens were kept in the chamber until final hyoid manipulation to allow maximal rehydration.

Specimen Staining

For diceCT staining, two solutions of Lugol's Iodine were prepared. For the specimen with the hyoid apparatus in the relaxed dewlap position, a solution of 2.5% weight-by-volume (w/v) Lugol's Iodine (I_2KI) was prepared, and the specimen was stained for three weeks. For the specimen with the dewlap in the extended position, a solution of 2% w/v Lugol's Iodine was prepared, and the specimen was stained for two weeks. These concentrations and staining times were chosen due to the differential sizes of the specimens to avoid overstaining.

Manipulation of Hyoid Apparatus

Because the skin of the dewlap did not regain elasticity during rehydration, it was physically removed. This did not affect the primary scope of the study, as the musculature does not insert on the skin and can be studied without the dewlap integument. To achieve extension, the brace harness was placed around the lower torso (immediately anterior to the hind limbs), with the inserted filament used to gently displace the second ceratobranchials into the extended position. With the current predominant models of dewlap extension finding the anole hyoid bones to function as a lever, the repositioning of second ceratobranchials was intended to replicate the lifelike extended position for the other bones of the hyoid apparatus, as well as the associated

musculature. For added support during staining and specimen transport, surgical suture was tied around the brace harness and the filament (Figure 2.3).

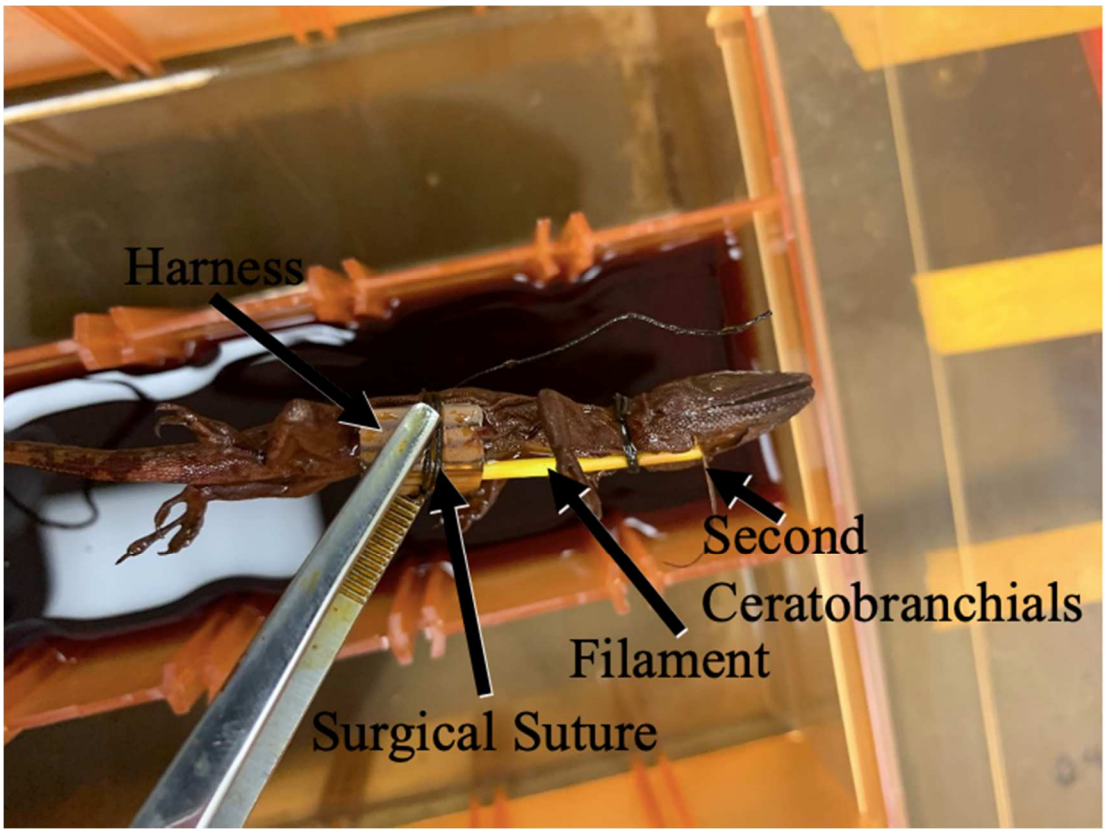

Figure 2.3. *Representation of brace harness on specimen.* Specimen undergoing diceCT staining process with hyoid bones extended. Observable here are the printed harness (brown), the 3D printer filament (yellow), and surgical suture (black). Projected second ceratobranchials can observed against the right tip of the 3D printed filament.

Scanning

Scanning of the specimens was performed at the MicroCT Imaging Consortium for Research and Outreach (MICRO) at the University of Arkansas in Fayetteville, Arkansas, using a Nikon XTH 225 ST with a rotating target head (Nikon Metrology, United Kingdom). Scan parameters for the relaxed specimen were 220 kV, 47 µA, with a voxel size of 0.01065 mm, and a 0.125 mm copper filter (Table 1). Scan parameters for the extended specimen were 220 kV, 47 µA, a voxel size of 0.01066 mm, and a 0.125

mm copper filter (Table 1). Scan parameters were set to optimize the scan quality based on the sizes of the specimens.

Table 2.1. *Specimen scan parameters.* Scan parameters for the relaxed and extended specimens analyzed in this study.

	Exemplar Relaxed Specimen	**Exemplar Extended Specimen**
kV	220	220
µA	47	47
Voxel Size	0.01065	0.01066
Cu Filter (mm)	0.125	0.125

Avizo Segmentation

Image stacks were exported as TIFF files. TIFF stacks of the CT data were imported into Avizo Lite 2021 (Thermofisher Scientific; Massachusetts) for digital dissection of the anole ventral craniocervical musculature. Gray scale and sharpening filters were not applied. Muscles were hand-segmented using a combination of the lasso tool (drawn every five slices, with interpolation to fill intermediate space), and the magic wand tool.

Results: Digital Dissection

Hyoid Skeleton

The hyoid apparatus itself is comprised of five paired elements and two unpaired elements (Figure 2.4). These elements include the hyoid body, the entoglossal process, the hypohyals, the ceratohyals, the epihyals, first ceratobranchials, epibranchials, and second ceratobranchials.

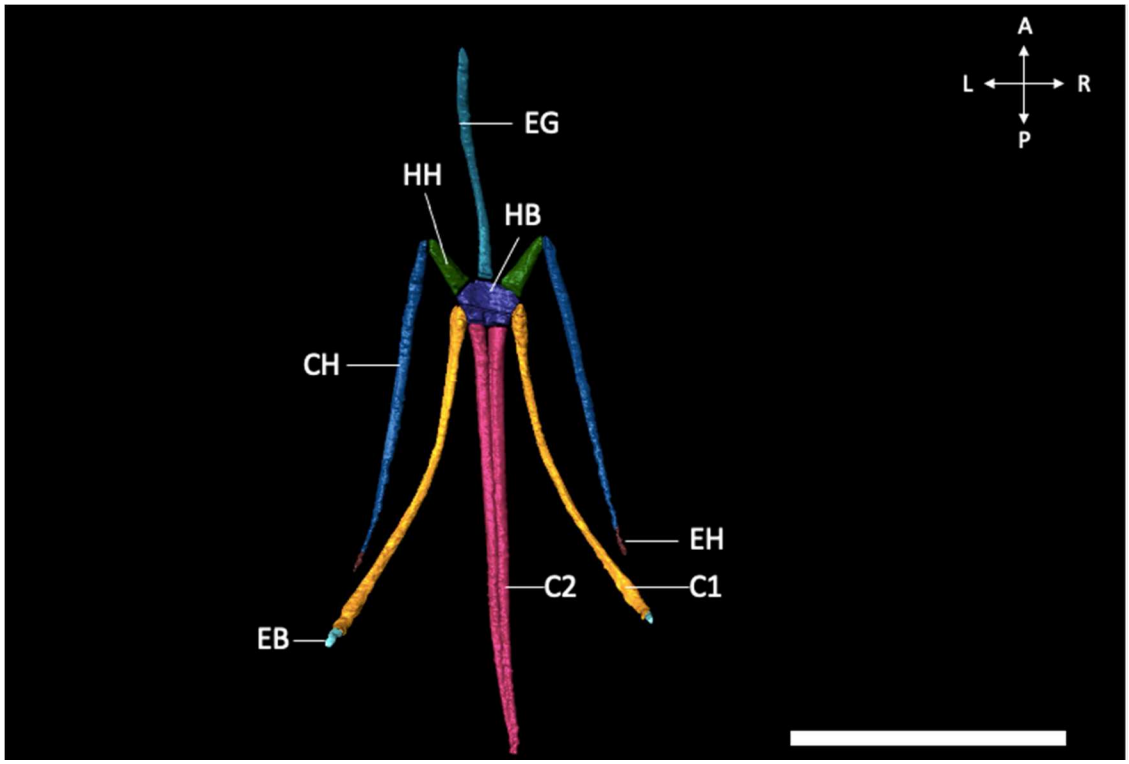

Figure 2.4. *Anole hyoid apparatus.* Digitally dissected hyoid apparatus of *Anolis carolinensis* in dorsal view. Ceratohyal (Dark Blue; CH), First Ceratobranchial (Orange; C1), Second Ceratobranchial (Magenta; C2), Epibranchial (Light Blue; EB), Entoglossal Process (Turquoise; EG), Epihyal (Brown; EH), Hyoid Body (Purple; HB), Hypohyal (Dark Green; HH). Scale bar = 5 mm. Compass rose orientations: Anterior (A), Posterior (P), Left (L), Right (R).

Hyoid Body

The hyoid body is the central element of the hyoid apparatus to which the entoglossal process, hypohyals, first ceratobranchials, and second ceratobranchials attach (Figure 2.4). It is dorsally compressed and laterally elongated in cross section.

Entoglossal Process

The entoglossal process is a long, thin, unpaired element projecting anteriorly from anterior aspect of the midline of the hyoid body (Figure 2.4). The entoglossal element is circular in cross-section. It is continuous with the hyoid body.

Hypohyals

The hypohyals are short, paired elements that project anterolaterally from the hyoid body (Figure 2.4). They attach to the ceratohyals at their distal aspect. The hypohyals are dorsally compressed and ovoid in cross section.

Ceratohyals

The ceratohyals are long, thin paired elements that project posterolaterally from their attachment to the distal aspect of the hypohyals (Figure 2.4). The ceratohyals are attached to the epihyals at their distal aspect and are circular in cross section.

Epihyals

The epihyals are small, paired elements that attach to the distal tips of the ceratohyals (Figure 2.4). They are oriented and project dorsally from their attachment to the ceratohyals on their posterior aspect.

First Ceratobranchials

The first ceratobranchials are long, thin paired elements that project posterolaterally from the posterior aspect of the hyoid body (Figure 2.4). They attach to the epibranchials at their distal aspect and are circular in cross section.

Epibranchials

The epibranchials are small, paired elements that attach to the distal tips of the first ceratobranchials (Figure 2.4). They are oriented and project dorsally from their attachment to the first ceratobranchials.

Second Ceratobranchials

The second ceratobranchials are long, thin paired elements that project posteriorly from the midline of the hyoid body (Figure 2.4). They are circular in cross section and are continuous with the hyoid body.

Hyoid Apparatus- Relaxed vs Extended

In the relaxed position, the elements of the hyoid apparatus lie horizontally along the ventral aspect of the gular region in line of the ventral aspect of the gular region and each other (Figure 2.5a). The second ceratobranchials project directly posterior, toward the sternum. In the extended position (Figure 2.5b), the first ceratobranchial, epibranchial, and second ceratobranchial elements have shifted. They are displaced as follows: 1) the first ceratobranchials are displaced superiorly to the other hyoid elements; 2) the epibranchials are displaced superiorly with the first ceratobranchials; 3) the second ceratobranchials are displaced ventrally; 4) the hypohyals are keeled ventrally; and 5) the proximal aspect of the entoglossal process is depressed.

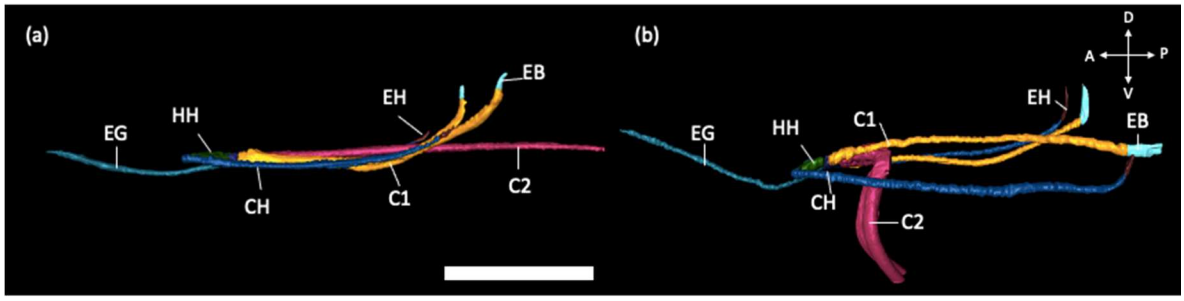

Figure 2.5. *Anole hyoid apparatus: relaxed vs extended.* Digitally dissected *Anolis carolinensis* hyoid apparatus in relaxed (a) and extended (b) positions, from the lateral aspect. Ceratohyal (Dark Blue; CH), First Ceratobranchial (Orange; C1), Second Ceratobranchial (Magenta; C2), Epibranchial (Light Blue; EB), Entoglossal Process (Turquoise; EG), Epihyal (Brown; EH), Hyoid Body (Purple; HB), Hypohyal (Dark Green; HH). Scale bar = 5 mm. Compass rose orientations: Anterior (A), Posterior (P), Dorsal (D), Ventral (V).

M. Ceratohyoideus

The *M. ceratohyoideus* is a long, thin, bilaterally paired muscle in *A. carolinensis* (Figure 2.6). The *M. ceratohyoideus* attaches to the medial aspect of the ceratohyal element and has a second attachment site into the lateral aspect of the first ceratobranchial element (Table 2). It is intrinsic to the hyoid apparatus. The *M. ceratohyoideus* is broadest at its midpoint, and tapers along each of its edges toward both

the base of the ceratohyal and first ceratobranchial as well as toward the distal ends of both bones.

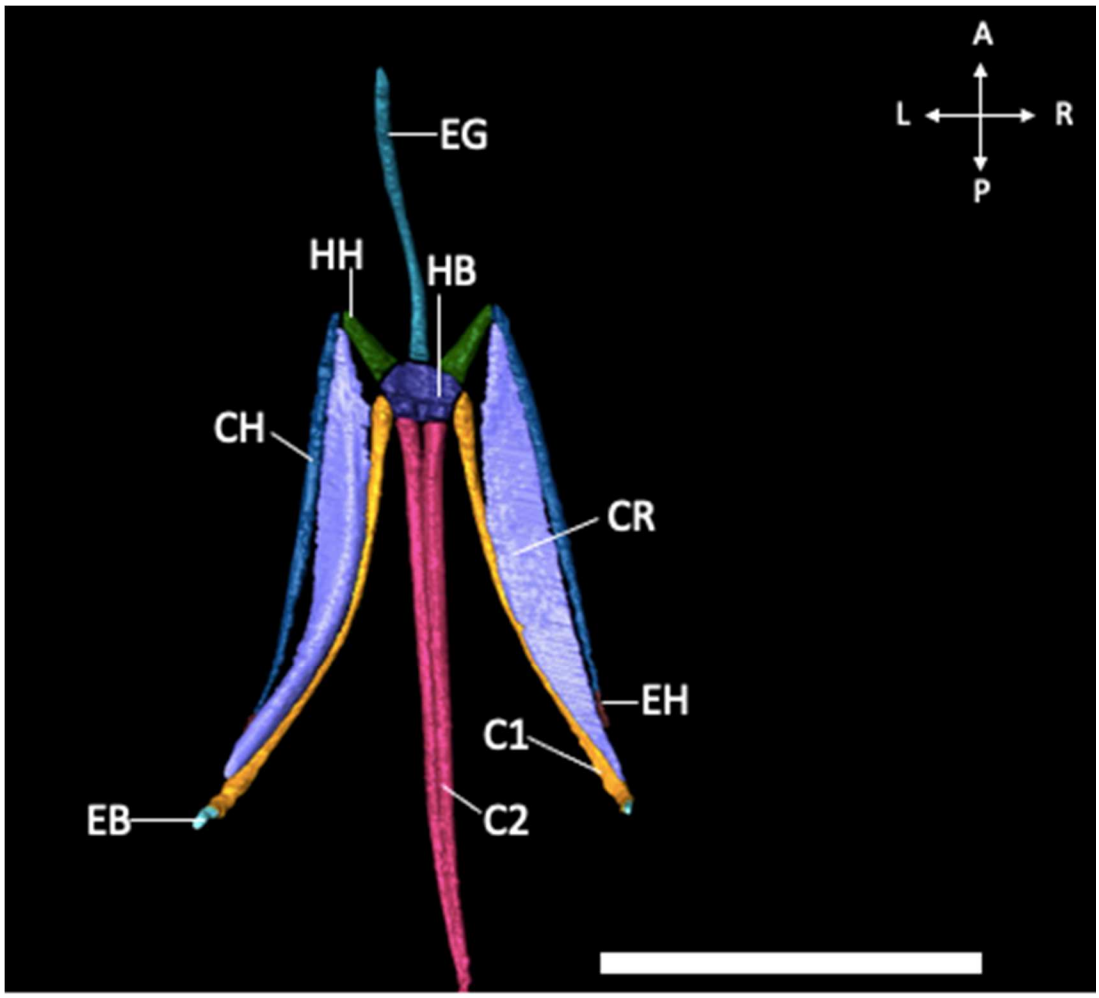

Figure 2.6. *Anole M. ceratohyoideus.* Digitally dissected *M. ceratohyoideus* (lavender) in the relaxed dewlap position, depicting its relationship with the hyoid apparatus from dorsal view. Ceratohyal (Dark Blue; CH), First Ceratobranchial (Orange; C1), Second Ceratobranchial (Magenta; C2), *M. ceratohyoideus* (CR; Lavender), Epibranchial (Light Blue; EB), Entoglossal Process (Turquoise; EG), Epihyal (Brown; EH), Hyoid Body (Purple; HB), Hypohyal (Dark Green; HH). Scale bar = 5 mm. Compass rose orientations: Anterior (A), Posterior (P), Left (L), Right (R).

M. ceratohyoideus- Relaxed vs Extended Positions

When the hyoid apparatus is in the relaxed dewlap position (Figure 2.7a), the *M. ceratohyoideus* sits flattened, with the muscle following the orientation of the first ceratobranchial and ceratohyals. In the extended dewlap position (Figure 2.7b), the

medial aspect of the *M. ceratohyoideus* is displaced dorsally with the first ceratobranchial bone, with the lateral aspect remaining more ventral with the unmoved ceratohyal.

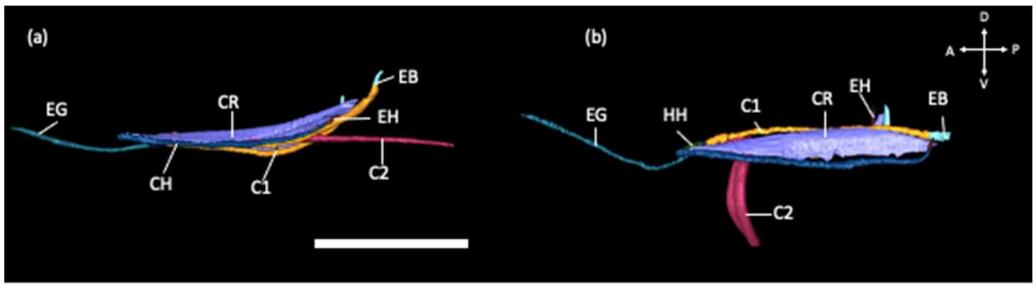

Figure 2.7. *Anole M. ceratohyoideus: relaxed vs extended.* Digitally dissected *M. ceratohyoideus* (lavender) in the relaxed (a) and extended (b) dewlap positions, depicting its relationship with the hyoid apparatus from lateral view. Ceratohyal (Dark Blue; CH), First Ceratobranchial (Orange; C1), Second Ceratobranchial (Magenta; C2), *M. ceratohyoideus* (CR; Lavender), Epibranchial (Light Blue; EB), Entoglossal Process (Turquoise; EG), Epihyal (Brown; EH), Hyoid Body (Purple; HB), Hypohyal (Dark Green; HH). Scale bar = 5 mm. Compass rose orientations: Anterior (A), Posterior (P), Dorsal (D), Ventral (V).

M. hyoglossus

The *M. hyoglossus* is a long, tubular, bilaterally paired muscle in *Anolis carolinensis* (Figure 2.8). The *M. hyoglossus* attaches to the lateral aspect of the first ceratobranchial before a second attachment into and running through the length of the tongue (Table 2.2). It expands along its length ventrally and laterally, reaching a maximum breadth and circumference near the midpoint of its length, before narrowing and tapering toward the tip of the tongue.

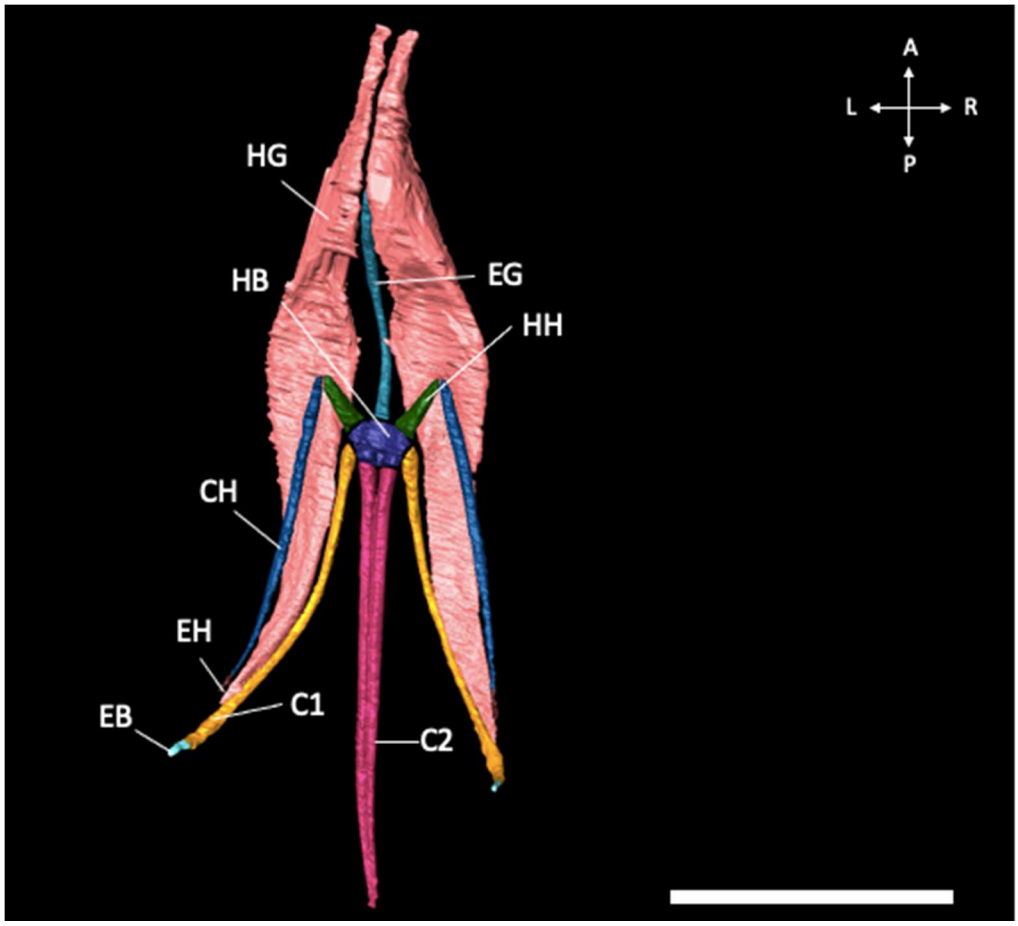

Figure 2.8. *Anole M. hyoglossus.* Digitally dissected *M. hyoglossus* (pink) in the relaxed dewlap position, depicting its relationship with the hyoid apparatus from dorsal view. Ceratohyal (Dark Blue; CH), First Ceratobranchial (Orange; C1), Second Ceratobranchial (Magenta; C2), *M. hyoglossus* (HG; pink), (CR; Lavender), Epibranchial (Light Blue; EB), Entoglossal Process (Turquoise; EG), Epihyal (Brown; EH), Hyoid Body (Purple; HB), Hypohyal (Dark Green; HH). Scale bar = 5 mm. Compass rose orientations: Anterior (A), Posterior (P), Left (L), Right (R).

M. hyoglossus- Relaxed vs. Extended Positions

When the hyoid apparatus is in the relaxed dewlap position (Figure 2.9a), the hyoglossus is parallel to the ventral surface of the oral floor. It elevates slightly from its origin on the first ceratobranchial upon entering tongue and remains level through the extent of its length. When the hyoid apparatus is in the extended dewlap position (Figure 2.9b), the anterior division of the *M. hyoglossus* remains undeformed, but the posteromedial division (along the first ceratobranchial), is displaced vertically with the bone.

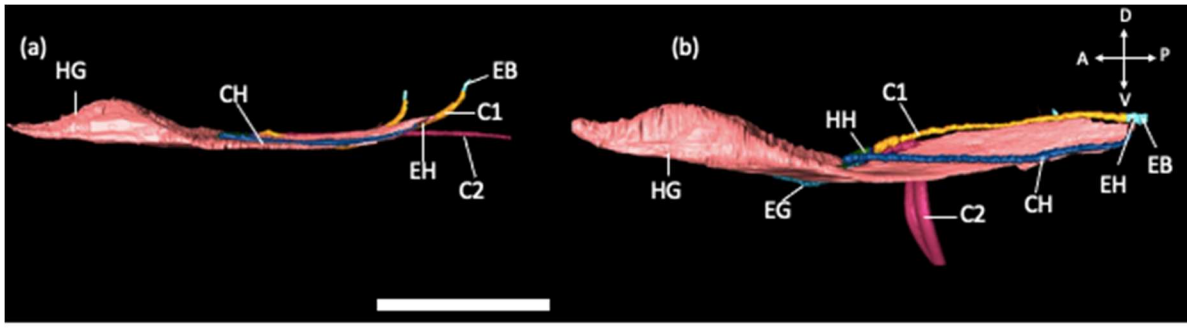

Figure 2.9. *Anole M. hyoglossus: relaxed vs extended.* Digitally dissected *M. hyoglossus* (pink) in the relaxed (a) and extended (b) dewlap position, depicting its relationship with the hyoid apparatus from lateral view. Ceratohyal (Dark Blue; CH), First Ceratobranchial (Orange; C1), Second Ceratobranchial (Magenta; C2), *M. hyoglossus* (HG; pink), (CR; Lavender), Epibranchial (Light Blue; EB), Entoglossal Process (Turquoise; EG), Epihyal (Brown; EH), Hyoid Body (Purple; HB), Hypohyal (Dark Green; HH). Scale bar = 5 mm. Compass rose orientations: Anterior (A), Posterior (P), Dorsal (D), Ventral (V).

M. omohyoideus

The *M. Omohyoideus* is a long, thin, bilaterally paired muscle in *A. carolinensis* (Figure 2.10). The *M. omohyoideus* attaches to the anterior dorsal aspect of the scapula before wrapping anteromedially to the ventral aspect of the craniocervical region. On the hyoid apparatus, it attaches to the posterior aspect of the first ceratobranchial (Table 2) and onto the hyoid apparatus superficially to the *M. Sternohyoideus* (see section *M. sternohyoideus*).

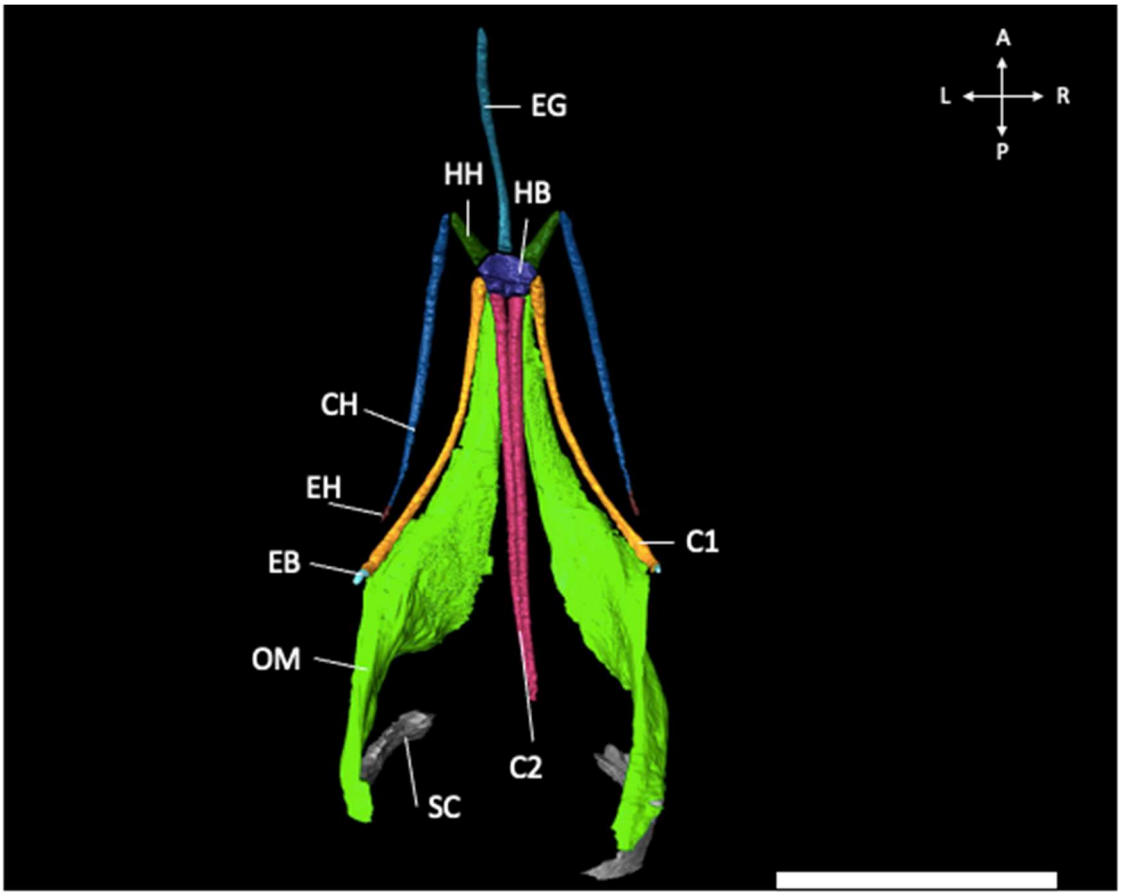

Figure 2.10. *Anole M. omohyoideus.* Digitally dissected *M. omohyoideus* (Light Green) in the relaxed dewlap position, depicting its relationship with the hyoid apparatus and the scapula (Grey; SC) from dorsal view. Ceratohyal (Dark Blue; CH), First Ceratobranchial (Orange; C1), Second Ceratobranchial (Magenta; C2), Epibranchial (Light Blue; EB), Entoglossal Process (Turquoise; EG), Epihyal (Brown; EH), Hyoid Body (Purple; HB), Hypohyal (Dark Green; HH), *M. Omohyoideus* (Light Green; OM), Scapula (SC). Scale bar = 5 mm. Compass rose orientations: Anterior (A), Posterior (P), Left (L), Right (R).

M. omohyoideus- Relaxed vs Extended Positions

When the hyoid apparatus is in the relaxed dewlap position (Figure 2.11a), the *M. omohyoideus* runs anteroventrally from the scapula to the ventral cervical region. The muscle is laterally compressed until it begins to wrap onto the ventral aspect of the cervical region, where it transitions to vertically compressed. The structure remains flattened and is aligned with the hyoid apparatus along its insertion into the first ceratobranchial. When the hyoid apparatus is in the extended dewlap position (Figure 2.11b), the muscle becomes highly folded near the hyoid apparatus in association with

the displaced first ceratobranchials. Following the structure to its origin on the scapula, deformation decreases.

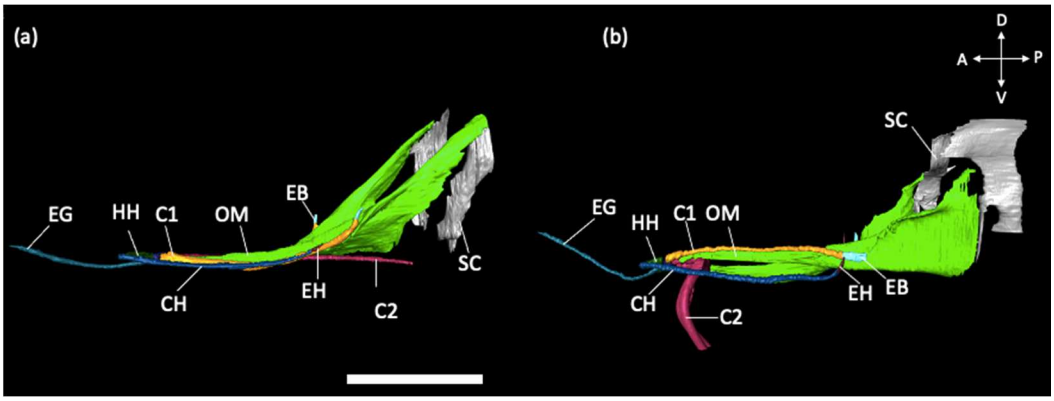

Figure 2.11. *Anole M. omohyoideus: relaxed vs extended.* Digitally dissected *M. omohyoideus* (light green) in the relaxed (a) and extended (b) dewlap position, depicting its relationship with the hyoid apparatus from lateral view. Ceratohyal (Dark Blue; CH), First Ceratobranchial (Orange; C1), Second Ceratobranchial (Magenta; C2), *M. Omohyoideus* (OM; light green), (CR; Lavender), Epibranchial (Light Blue; EB), Entoglossal Process (Turquoise; EG), Epihyal (Brown; EH), Hyoid Body (Purple; HB), Hypohyal (Dark Green; HH), Scapula (Gray; SC). Scale bar = 5 mm. Compass rose orientations: Anterior (A), Posterior (P), Dorsal (D), Ventral (V).

M. sternohyoideus

The *M. sternohyoideus* is a long, thin, sheet-like muscle in *A. carolinensis*, positioned on the ventral aspect of the cervical region (Figure 2.12). The *M. sternohyoideus* attaches to the anteroventral aspect of the sternum, before proceeding anteriorly along the ventral aspect of the cervical region. The *M. sternohyoideus* broadens anteriorly before being constrained along its lateral aspect by the *M. omohyoideus*. It the attaches to the posterior aspect of the first ceratobranchial and tapers laterally with the medially convex curvature of the first ceratobranchial, before an additional insertion onto the hyoid body (Table 2). The *M. sternohyoideus* inserts onto the hyoid apparatus immediately deep to the *M. omohyoideus*.

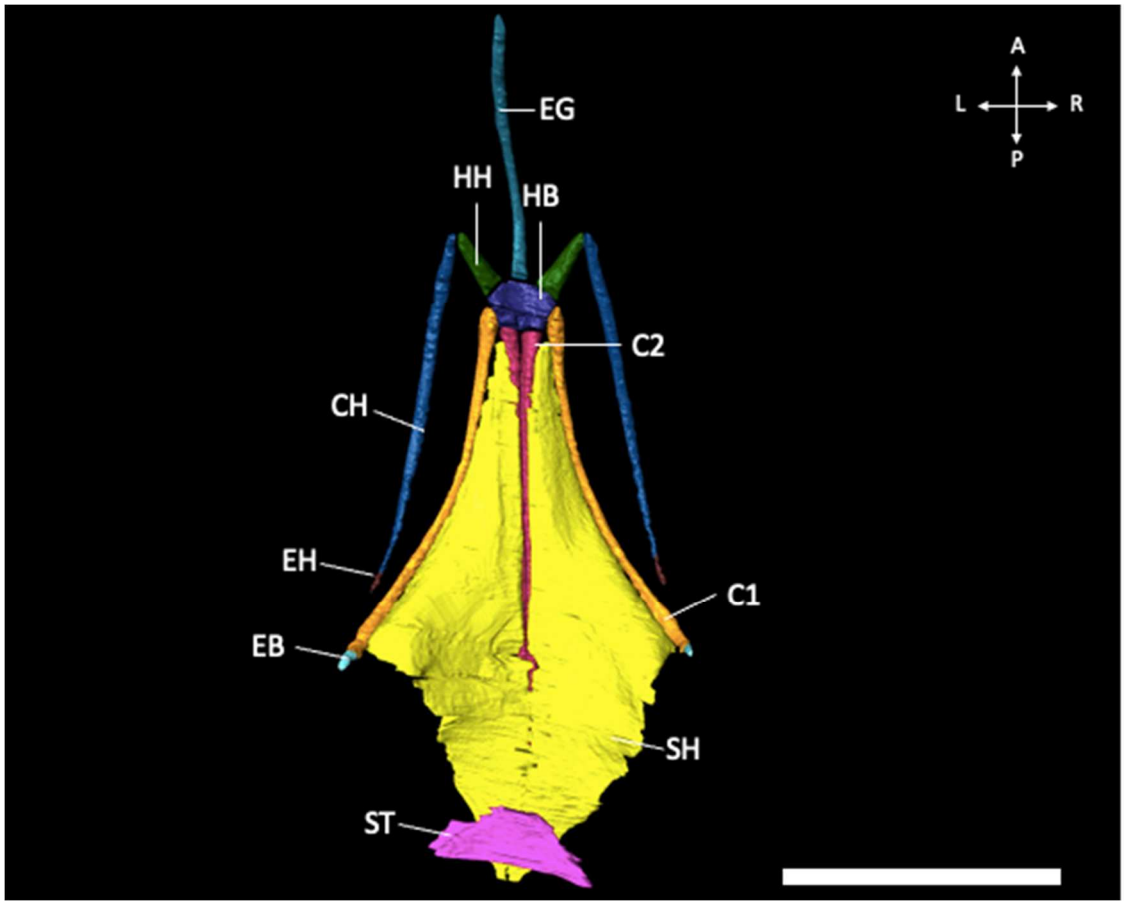

Figure 2.12. *Anole M. sternohyoideus.* Digitally dissected *M. sternohyoideus* (yellow) in the relaxed dewlap position, depicting its relationship with the hyoid apparatus and the scapula (bright pink) from dorsal view. Ceratohyal (Dark Blue; CH), First Ceratobranchial (Orange; C1), Second Ceratobranchial (Magenta; C2), *M. sternohyoideus* (SH; yellow), *M. ceratohyoideus* (CR; Lavender), Epibranchial (Light Blue; EB), Entoglossal Process (Turquoise; EG), Epihyal (Brown; EH), Hyoid Body (Purple; HB), Hypohyal (Dark Green; HH), sternum (Bright Pink; ST). Scale bar = 5 mm. Compass rose orientations: Anterior (A), Posterior (P), Left (L), Right (R).

M. sternohyoideus- Relaxed vs Extended Positions

In the relaxed dewlap position, the *M. sternohyoideus* lies flattened and parallel to the orientation of the hyoid apparatus (Figure 2.13a). In the extended dewlap position, the *M. sternohyoideus* is relatively undeformed (Figures 2.13b). This is in exception to the anterior aspect, which is folded and displaced along its insertion to the first ceratobranchial.

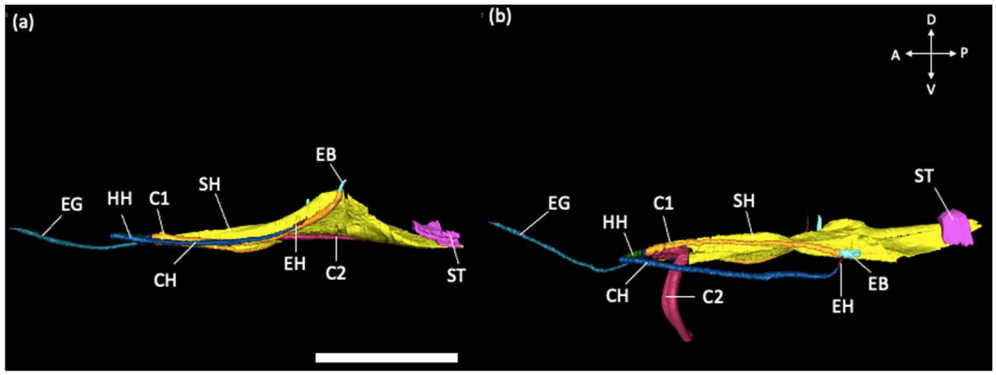

Figure 2.13. *Anole M. sternohyoideus: relaxed vs extended.* Digitally dissected *M. sternohyoideus* (yellow) in the relaxed (a) and extended (b) dewlap position, depicting its relationship with the hyoid apparatus from lateral view. Ceratohyal (Dark Blue; CH), First Ceratobranchial (Orange; C1), Second Ceratobranchial (Magenta; C2), *M. sternohyoideus* (SH; yellow), Epibranchial (Light Blue; EB), Entoglossal Process (Turquoise; EG), Epihyal (Brown; EH), Hypohyal (Dark Green; HH), Sternum (Bright Pink; ST). Scale bar = 5 mm. Compass rose orientations: Anterior (A), Posterior (P), Dorsal (D), Ventral (V).

Table 2.2. *Hyoid musculature attachment sites.* Highlighted musculature with identified attachment sites.

Muscle	Attachment Site 1	Attachment Site 2
M. Ceratohyoideus	Medial aspect of ceratohyal	Lateral aspect of first ceratobranchial
M. Hyoglossus	Lateral aspect of first ceratobranchial	Body of the tongue
M. Omohyoideus	Medial aspect of first ceratobranchial	Antero-dorsal aspect of scapula
M. Sternohyoideus	Medial aspect of the first ceratobranchial	Antero-ventral aspect of the sternum

Discussion

My aim for this part of my thesis was to digitally dissect the musculoskeletal structures implicated in the Anole dewlap action *in situ*, in both extended and relaxed positions (Figures 2.14; 1.15; 2.16). To accomplish this a combination of diceCT, digital imaging, and 3D printing methods were employed. These methods allowed for a novel, direct comparison of the hyoid apparatus and associated musculature in each position.

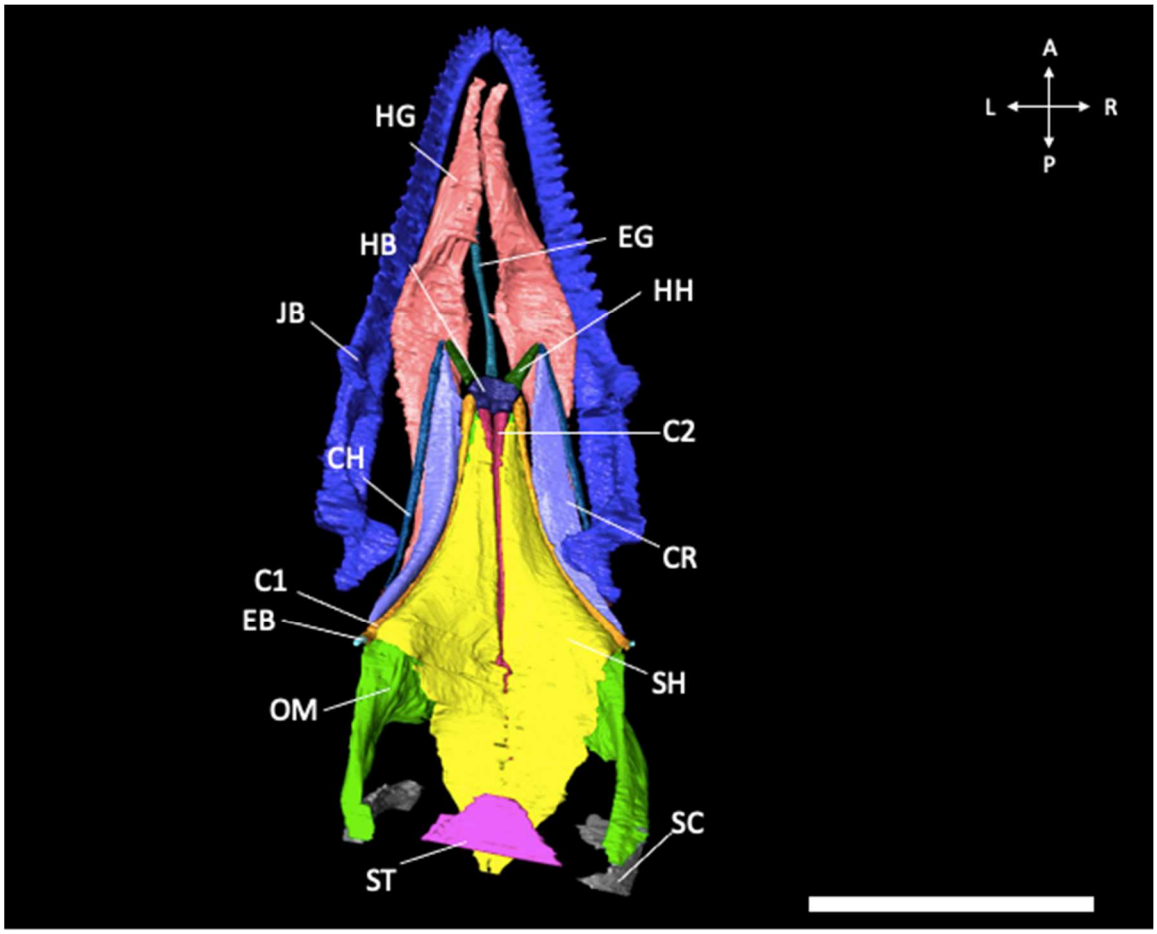

Figure 2.14. *Anole hyoid musculature: dorsal view.* Full digital dissection of implicated dewlap extension muscles and reference structures in relaxed position from dorsal view. Structures displayed are the Ceratohyal (Dark Blue; CH), First Ceratobranchial (Orange; C1), Second Ceratobranchial (Magenta; C2), *M. ceratohyoideus* (Lavender; CR), *M. hyoglossus* (HG; pink), *M. omohyoideus* (light green; OM) *M. sternohyoideus* (Yellow; SH), Epibranchial (Light Blue; EB), Entoglossal Process (Turquoise; EG), Epihyal (Brown; EH), Hyoid Body (Purple; HB), Hypohyal (Dark Green; HH), Jaw Bones (Blue; JB), Scapula (Gray; SC), Sternum (Bright Pink; ST). Scale bar = 5 mm. Compass rose orientations: Anterior (A), Posterior (P), Left (L), Right (R).

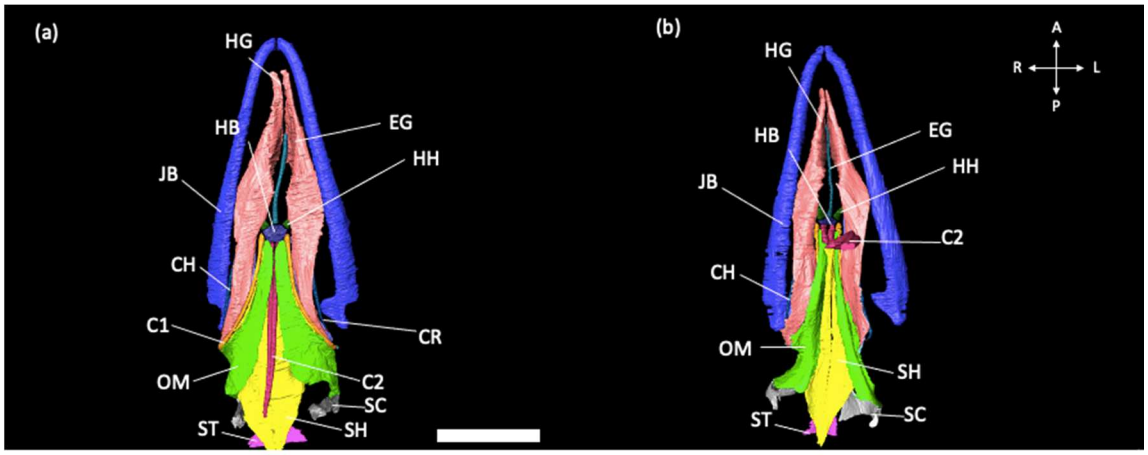

Figure 2.15. *Anole hyoid musculature: relaxed vs extended, ventral view.* Full digital dissection of implicated muscles and reference structures in (a) relaxed and (b) extended positions from ventral view. Structures displayed are the Ceratohyal (Dark Blue; CH), First Ceratobranchial (Orange; C1), Second Ceratobranchial (Magenta; C2), *M. ceratohyoideus* (Lavender; CR), *M. hyoglossus* (HG; pink), *M. omohyoideus* (light green; OM) *M. sternohyoideus* (Yellow; SH), Epibranchial (Light Blue; EB), Entoglossal Process (Turquoise; EG), Epihyal (Brown; EH), Hyoid Body (Purple; HB), Hypohyal (Dark Green; HH), Jaw Bones (Blue; JB), Scapula (Gray; SC) Sternum (Bright Pink; ST). Scale bar = 5 mm. Compass rose orientations: Anterior (A), Posterior (P), Left (L), Right (R).

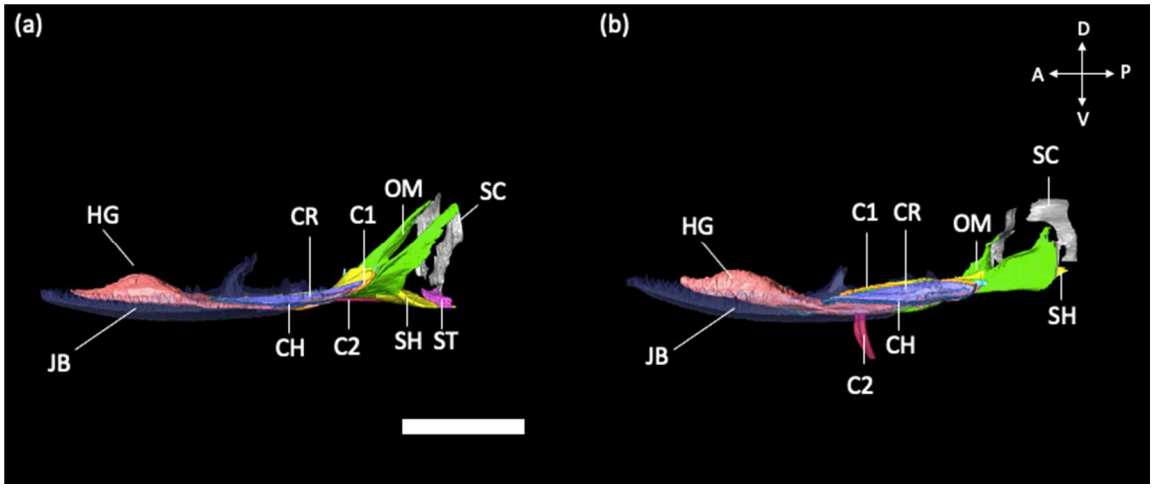

Figure 2.16. *Anole hyoid musculature: relaxed vs extended, lateral view.* Full digital dissection of implicated muscles and reference structures in (a) relaxed and (b) extended positions from lateral view. The jawbone has been rendered transparent for easier observation of structures of interest. Structures displayed are the Second Ceratobranchial (Magenta; C2), *M. hyoglossus* (HG; pink), *M. omohyoideus* (light green; OM) *M. sternohyoideus* (Yellow; SH), Jaw Bones (Blue; JB), Scapula (Gray; SC) Sternum (Bright Pink; ST). Scale bar = 5 mm. Compass rose orientations: Anterior (A), Posterior (P), Left (L), Right (R).

Of the muscle deformation and repositioning that resulted from extension of the second ceratobranchials, that of the *M. ceratohyoideus* is noteworthy. Intrinsic to the hyoid apparatus (Figure 2.6), this muscle presents the most observable transition out of the other 4 muscles implicated muscles in dewlap extension (Figure 2.7). The entire length of the *M. ceratohyoideus* is displaced during extension, and this observation aligns with previous studies that identify the *M. ceratohyoideus* as a primary driver of the dewlap opening mechanism (Bels, 1990; Font and Rome, 1990).

Of the remaining muscles that were targeted for digital dissection, minimal deformation was observed in the *M. hyoglossus* in extension (Figure 2.9). This slight movement is observed on the posterior aspect of the muscle, with no observable changes occurring in the overall positioning of the muscle, as posited by C. P. Gnanamuthu (1937). This suggests that the involvement of the *M. hyoglossus* during dewlap extension is unlikely. Small shifts were observed between the *M. sternohyoideus* and *M. omohyoideus* during dewlap extension (Figure 2.11; 2.13). Both muscles remained minimally deformed toward their origins on the sternum and scapula respectively. As they progress anteriorly toward their insertion on the hyoid apparatus, each muscle becomes increasingly deformed and folded. With this observation, the response of the *M. sternohyoideus* and *M. omohyoideus* appears to be reactive to the displacement of the hyoid apparatus, as opposed to being a primary driver of extension.

However, the displacement of the *M. sternohyoideus* and *M. omohyoideus* also does present the possibility that these muscles should be reconsidered as a functional unit in the dewlap opening mechanism. Although appearing to conflict with the most recent prior studies (Bels, 1990; Font and Rome, 1990), the pattern of deformation of these

muscles during extension suggests that they participate in the extension mechanism. In this potential model, the *M. sternohyoideus*, *M. omohyoideus*, and *M. ceratohyoideus* act in concert to swing the second ceratobranchials into the extended position. Future work on the anole dewlap should continue to reanalyze the role of the *M. sternohyoideus* and *M. omohyoideus* in the dewlap extension mechanism.

The observations in this digital dissection support the conclusions of Font and Rome (1990) and Bels (1990): the *M. ceratohyoideus* is a primary driver of dewlap extension. Interestingly, this aligns with the evolutionary origins of the muscle. In urodeles, a homologous muscle, the *M. branchiohyoideus*, is involved in moving the gills, meaning in both instances these muscles are involved in intrinsic action of pharyngeal arch derived structures (Lauder and Shaffer, 1988). The observed displacement of the first ceratobranchials aligns with the Bels (1990) model of extension, as opposed to the Font and Rome model, which only implicates displacement of the ceratohyals while the first ceratobranchials remain fixed. However, as opposed to a ventral displacement, as interpreted by Bels, our model led to a dorsal displacement of the first ceratobranchial. With these observations, this modified mechanism action potentially merits a revisit of the interpretation of the anole hyoid apparatus acting as first-order lever during the dewlap opening mechanism.

A limitation to our study is the sample size. One specimen was fully analyzed in each position, limiting the number of observations that could be performed. Future goals are to diceCT stain and observe more specimens in the extended and relaxed positions to confirm that our brace harnesses provide consistent muscle deformation and modification. Another limitation of this study was the fixation of the specimens, leading

to a loss of the natural mobility of the targeted muscles. Future goals also include repeating these analyses with fresher, unfixed specimens to decrease limitations of muscle manipulation. The displacement of the entoglossal process during extension also implicates the *M. verticalis*, which surrounds the entoglossal process in squamates (Zghikh et al, 2014), as a prospective target muscle for future work on anole dewlap action. Another future direction is the use of visual imaging methods such as X-Ray of Moving Morphology (XROMM: Brainerd et al, 2010), to further resolve these form and function relationships by being able to observe the displacement of the hyoid elements during extension in live specimens (including agonist and antagonist muscle actions), followed by analysis with the diceCT imaging and digitally segmented models (Orsbon et al, 2018). Additionally, and because dewlaps only appear within the Iguania (Ord et al, 2015), detailed analysis of these structures morphologically and functionally is essential to understanding their evolution through time and the role they have played in iguanian diversification. This future work will help build on the groundwork of this study in understanding the anole dewlap mechanism through modern methods, and further our understanding of how this mechanism directly relates to their behavior, ecology, and evolution.

CHAPTER III

HISTOLOGY OF THE SKELETAL ELEMENTS OF THE ANOLE HYOID APPARATUS

Introduction

While many analyses of the function, performance, fitness paradigm focus on gross anatomical structures (Arnold 1983), an understanding of microanatomy at the structural and cellular levels is equally important. Animals have a variety of complex tissues, including "soft tissues" (such as muscles, skin, and nervous tissue), and rigid structures (Nikolov et al, 2011; Dubois 2014; Schiltuizen et al, 2006), or "hard tissues," such as the internal skeleton of vertebrates. The vertebrate skeletal system is integrated with the muscular system (Hirasawa and Kuratani, 2015; Watkins. 2014), but its constituents are classified as connective tissues, primarily in the form of cartilage and bone (Ogston, 1875; Baber, 1855; Paget, 1855; Hoggan and Hoggan, 1880; Stump, 1925; Watkins, 2014). Cartilage is connective tissue with a primary cellular composition of chondrocytes (Kraus, 2006), and it is thought to have originated earlier than bone evolutionarily, with fossils of the earliest fishes having skeletons composed of cartilage (Janvier, 1999). Cartilage remains the predominant component of the internal skeleton in cyclostomes (lampreys and hagfish; Robson et al, 1997) and chondrichthyans (sharks, rays, and relatives; Seidel et al, 2021). However, in many Osteichthyans (e.g., bass, catfish, drum), ossified bone is predominant, comprising most of the skeleton (Hirasawa and Kuratani,

2015). This osseous skeletal composition has been retained in tetrapods, with cartilaginous skeletal elements primarily becoming ossification centers promoting the development of ossified bone in a process known as endochondral ossification (Hirasawa and Kuratani, 2015).

Cartilage and bone have multiple similarities at the histological level, but their organization differs substantially regarding mineralization. For example, both have organic matrices that are composed of collagens (Bruckner and van der Rest, 1994; Wang et al, 2001), glycosaminoglycans (Mankin and Lipiello, 1971; Vejlens 1970), proteoglycans (Roughley, 2006; Lamoureux et al, 2007), and adhesive proteins (Tsai et al, 2007; Gu et al, 1999). The extracellular matrices of each tissue are extensive, and suspend cells embedded within small, oblong spaces in the tissue called lacunae. Both also grow via mesenchymal progenitor cells (Kraus, 2006). In cartilage, the mature embedded cells are primarily chondrocytes, with chondroblast progenitor cells that deposit new tissue (Kraus, 2006). In bone, the mature embedded cells are primarily osteocytes, with osteoblast progenitor cells that secrete new osteoid (Kraus, 2006). Bone has a third associated cell type: osteoclasts, which are derived from the monocyte-macrophage differentiation line (Nijweide et al, 1986), and are involved in the remodeling of bone by resorption (Feng and Teitelbaum, 2006). While cartilage is composed entirely of an organic matrix (Nagase and Kashiwagi, 2003), bone is constituted of both an organic and a mineralized inorganic matrix (Blair et al, 1986). The organic, un-mineralized matrix of cartilage allows for flexibility and a high capacity for deformation while maintaining structural integrity. The paired organic and inorganic matrix of bone allows for some flexibility with additional rigidity and support. Another

distinction is that cartilage is avascular (Fenwick et al, 1999) while bone is highly vascularized (Filipowska et al, 2017). Both cartilage and bone can function independently from one another to support body movement and structural integrity; however, they can also interact to form connective tissue compliments that facilitate novel functions (Watkins, 2014).

Three forms of cartilage are recognized: hyaline, elastic, and fibrocartilage. Hyaline cartilage is the most prevalent form in tetrapods, comprising the embryonic skeleton, articular cartilage, and portions of the respiratory tract. These hyaline cartilages typically display perichondrium, and have extracellular matrices composed of type II collagen and proteoglycans (Kheir and Shaw, 2009). Elastic cartilage in mammals is found in the external ear, while in other tetrapods it is present in the auditory canal and epiglottis. Compositionally, elastic cartilage is like hyaline cartilage, but with the addition of elastic fibers (Cox and Peacock, 1977). The final recognized cartilage is fibrocartilage, which is prominent in intervertebral disks and at the insertion points of ligaments and tendons of joints in most tetrapods. This cartilage form lacks perichondrium, is composed of type I collagen, and has lacunae organized in a linear arrangement (Benjamin and Evans, 1990).

Skeletal elements exist in multiple forms, usually with two major morphologies: long elements and flat elements (Tsuchiya et al, 1993). Long bones typically form via endochondral ossification, whereby the structure initially forms in hyaline cartilage, before being ossified (Mackie et al, 2008). Flat bones generally form by intramembranous ossification, whereby mesenchymal cell clusters develop into osteoblasts, forming ossification centers and eventually trabecular matrices and

periosteum generating the final skeletal element (Thompson et al, 2002). In Osteichthyans (including tetrapods), bone and cartilage interactions occur most predominantly at joints (Pierce et al, 2012). In these interactions, cartilage on the joint surfaces provides compressible padding, preventing bone on bone grinding (Arokoski et al, 2000). Cartilage and bone interactions can be exemplified by freely moving synovial joints, such as in the ulnocarpal joint (Kawashima et al, 2017) or the patellar joint (Lu et al, 2008). In these instances, paired bones are capped with hyaline cartilage and the articulation is surrounded by synovial-fluid-filled bursae and the dense connective tissue bands of ligaments and tendons (Khan et al, 2007). Ligaments connect bone to bone, adding support to joints, and tendons connect muscles to bone, allowing for movement about the joint in response to muscular extension or contraction (Amiel et al, 1984). Leverage for movement about an anatomical joint is achieved due to enthesis: the insertion of joint-associated soft tissues (ligaments, tendons, cartilage, fascia) onto bone (Apostolakos, 2014). In muscle-to-bone entheses, a clear transition from the cartilage attachment site to the tendon of the muscle can be observed histologically, with a fibrocartilage intermediate zone. Fibrocartilage is a specialized connective tissue comprised of cartilage as well as collagen fiber components, making it particularly tough and resilient, optimal for the stresses placed on attachment sites at joints (Benjamin and Evans, 1990). Attachment sites of tendons in ossified bones are associated with histological structures known as Sharpey's fibers (Benjamin et al, 2002). This is due to the insertion of the muscle's tendon into a hyaline cartilage interface, generating collagen fiber bundles that "burst" into the bone tissue (Benjamin et al, 2002). These bundles penetrate the subchondral bone, allowing the insertion to better resist the stresses of

muscular actions of contraction and extension. Multiple other types of joints exist, and can be classified by range of motion, anatomical composition, as well as plane of motion. Classification based on range of motion includes synarthrosis, wherein joints have a limited or negligible range of motion, such as sutures, amphiarthrosis, wherein joints have a limited range of motion, and diarthrosis, wherein joints have a full range of motion (Yavuz and Tuncer, 2020). Based on anatomical composition, joints can be fibrous, where neighboring bony elements are fixed, cartilaginous, where neighboring elements are joined by semi-flexible cartilage pads, or synovial, where neighboring elements are capped in hyaline cartilage and articulate within a lubricant-filled capsule (synovium), enabling complex motion. There are six types of synovial joints, which are named after the primary movement about the joint, including plane (Cammarata and Dahaer, 2012), hinge (Fuss, 1991), pivot (Natchev et al, 2015), condyloid (Barmakian, 1992), saddle (Gemeno et al, 2009), and ball-and-socket (Jaffar et al, 2016). A putative model for the study of morphology and histology of joints is the hyoid apparatus of squamates within the genus *Anolis*.

Squamates, such as the ecologically well-studied genus *Anolis* (Nicholson et al, 2007; Vanhooydonck et al, 2005; Vanhooydonck et al, 2009), represent an intriguing model for the observation of the interaction between cartilage and musculature. This is because the hyoid apparatus in squamates (Font and Rome 1990; Bels 1990; Gamble et al, 2008; Jones et al, 2009) is a composite structure at the tissue level, with elements comprised of both cartilage and bone, a condition that is conserved in *Anolis*, with the joints of the structure occurring between cartilage elements (Font and Rome 1990; Bels, 1990). The hyoid apparatus includes several examples of synovial-type-joints, which are

present in most terrestrial vertebrates allowing free movement. The hyoid apparatus is typically comprised of eight elements. There are two paired elements: the hyoid body and the entoglossal process; and six paired elements: the hypohyals, ceratohyals, epihyals, first ceratobranchials, epibranchials, and second ceratobranchials. These elements work together in squamates to support the tongue, open and close the airway, and promote swallowing. In many squamates, most of the hyoid apparatus is comprised of unmineralized hyaline cartilage (Li et al, 2018), as opposed to the condition observed in many mammals, wherein the hyoid elements are fully ossified (Shimizu et al, 2005). Many squamates also possess cartilaginous hyoid elements that are specialized for display behaviors, such as the anole dewlap, in which the second ceratobranchials of the hyoid extend into a tissue fold to open the dewlap fan (Bels, 1990; Font and Rome, 1990). In many anoles, the dewlap structure takes on peramorphic (extended period of developmental growth) morphology in males, being both larger and used more frequently in behavioral intra and interspecific interactions (Echelle et al, 1978). This leads to a hyoid apparatus that likely undergoes more strain in males than in females (Biewener, 1991). This structure also undergoes a distinctive sex-specific ontogenetic shift, with its development accelerating with increased testosterone (Lovern et al, 2001). This leads to a high potential for microanatomical variation between sexes and across ontogeny.

The histology of the anole hyoid apparatus was briefly described in both Font and Rome 1990 and Bels 1990 in conjunction with their analyses of the functional morphology of the dewlap protrusion mechanism. Font and Rome (using *A. equestris* as a model) found the first ceratobranchials to be the only components of the anole hyoid apparatus to be ossified, with a dorsoventrally compressed cross section. All remaining

components were described as cartilaginous. In each of these structures, the chondrocytes were organized into isogenous groups of four. Calcium deposits were present in the second ceratobranchial, and these were organized in semicircular patterns. Font and Rome (1990) found the chondrocytes to be organized into isogenous groups of four. For their tissue preparation, Font and Rome (1990) employed Milligan trichrome to distinguish muscles and connective tissue and Alizarin red staining to identify calcium deposits. Bels (using *A. carolinensis* as a model) also observed the first ceratobranchials to be the only mineralized component of the hyoid apparatus, with remaining structures concluded to be cartilaginous. However, Bels (1990) found the chondrocytes to be organized into isogenous groups of two or three. Both studies were congruent regarding the second ceratobranchials, wherein the mineralization was remarked to be in a semicircular pattern. Bels (1990) employed alizarin red and Alcian blue staining to identify calcium mineralization patterns. Bels (1990) also fixed is specimens in Bouin's solution saturated with calcium mitigate decalcification.

Specific Aims

I aim to provide a more detailed description of histology of the anole hyoid apparatus, including the nature of muscle attachment, as well as expanding the sample to multiple ontogenetic stages and using individuals of different sexes. These aspects are important to placing the anole hyoid apparatus into deep time evolutionary context, and to understand the structure and development of intricate, cartilage comprised tissues

Histological Staining & Meeting Specific Aims

An important method that is employed in histological analysis is tissue staining. By staining the tissues, additional details regarding tissue structure and composition can be

elucidated. A multitude of staining agents exist, and they differentially bind to different types of tissues based on cell types, organic compounds present, and cell morphology. Previous work in *Anolis* has included staining of the hyoid apparatus using Alcian blue, Alizarine red, and Milligan trichrome. Alcian blue is a staining agent that preferentially binds to polysaccharides (Scott et al, 1964); Alizarine red preferentially binds to calcium deposits (Puchtler et al, 1969); and Milligan's trichrome is used for staining muscles and collagens (Milligan, 1946). These staining strategies allowed for the distinguishing of the mineralization patterns along the different elements of the hyoid apparatus, particularly regions of cartilage from regions of calcification (Font and Rome, 1990; Bels, 1990). In this study, I introduce the application of Toluidine Blue to stain the anole hyoid apparatus. Toluidine Blue is a staining agent that can be used to identify cartilage, calcified elements, and calcification fronts (Williams, 1941). With this agent I aim to use histological preparation and staining protocols to examine sexual dimorphism and ontogeny at the tissue level in the context of the Anole hyoid apparatus.

Methods: Osteology of Hyoid Apparatus

Digital Segmentation

As outlined in Chapter 2 (section 2.7), the anole hyoid apparatus was digitally dissected for anatomical analysis by employing Avizo Lite digital imaging software (2020.1, Thermofisher, Massachusetts). Structures were manually segmented by a combination of the magic wand and paintbrush tools, while highlighting the bony structures of the hyoid every five to ten slices, followed by interpolation to form a continuous surface. These digital segmentations were used as a reference when defining the histology of the hyoid apparatus.

Methods: Histological Analysis

Obtaining Specimens

For this study, histological sections were made from six specimens of *A. carolinensis*. All specimens were obtained from Ward's Science (Rochester, New York), and were deceased when obtained with no capacity to preorder specimens of specific sexes or ontogenetic stages. The specimens were fixed in 10% neutral buffered formalin by Ward's Science. Because specimens were obtained as cadaveric materials, no IACUC protocol was required for this study. Of the six analyzed specimens, two were female, two were male, and two were juveniles. Mature male and female specimens were identified based off post-vent scale size and pattern (Lovern and Holmes, 2004). The smallest specimens in the sample were interpreted to be the youngest upon time of death (Goodman, 2010). The adult male specimens had snout-vent lengths (SVLs) of 5.35 cm and 5.00 cm; the female specimens had SVLs of 4.78 cm and 4.86 cm; and the putative juveniles had SVLs of 4.57 cm and 4.44 cm. The sex of the putative juvenile specimens was not observed or recorded for this study.

Specimen Preparation

Two preparation methods were employed for embedding:

1. For three specimens ($N_{Female} = 1$; $N_{Mmale} = 1$; $N_{juvenile} = 1$), the entire animal was embedded in Epothin2 (Buehler, Illinois Toolworks, Illinois). Specimens that were contorted during the preservation process were straightened and secured into position using tongue depressors as splints and paraffin wax. Slides prepared with this method will be referred to as "head".

2. For the other three specimens ($N_F = 1$; $N_M = 1$; $N_j = 1$), the hyoid was isolated via dissection. Hyoid isolation began dorsally with a deep, vertical incision posterior to the cranium through the cervical vertebrae and soft tissues of the neck until a plane the depth of the jaw joint was reached. An incision was then made laterally through the jaw joint to separate and remove the cranium, exposing the floor of the mouth and throat. Next, a shallow incision was made on the abdomen midway between the fore and hindlimbs on the ventral aspect. From this incision, the skin was removed anteriorly up to the mandibular symphysis to expose the second ceratobranchials, which lie directly beneath the skin. The hyoid musculature was then detached from the sternum. Finally, cuts were made along the interior edges of the jaws to detach them from the hyoid apparatus. This left only the hyoid apparatus, including musculature and tissues attached directly to it for embedding. Small, delicate structures that insert directly onto the hyoid were left associated so that attachment/insertion sites could be studied. Throughout this preparation, the hyoid apparatus was periodically soaked in formalin to prevent deformation of the hyoid bones. Slides prepared with this method will be referred to as "hyoid".

Embedding

Specimens were embedded in Epothin2 epoxy-based resin (Buehler, Illinois Toolworks, Illinois) prepared in a paper cup (1:1.43 ratio Epothin: catalyst). After thorough mixing, the resin was poured over specimens, which were held in appropriately sized containers. Epothin resin blocks were placed between the specimens and the container to ensure the specimens were completely immersed in the resin. Hyoids were glued onto the Epothin blocks using cyanoacrylate instant adhesive (Starbond Premium,

California) to prevent floating and repositioning of specimens while the resin set. All specimens and resin were then placed into a vacuum chamber to diminish pore spaces in the resin and to remove air bubbles. Following the vacuum chamber, the embedded specimens were placed in a refrigerator for 24 hours to allow the resin to set.

Cutting

Following embedding, hyoid-isolated specimens were cut into 2 cm thick wafers using an Isomet 1000 diamond embedded precision saw blade (Buehler, Illinois Toolworks, Illinois). Full body specimens were cut into 2 cm mm thick wafers using a water-cooled tile saw fitted with a continuous diamond blade tile saw fitted with a continuous rim diamond blade (Tilematic TS250X3, Husqvarna, Sweden). Cuts were made along anterior and posterior ends of the oral region of the embedded specimen, generating two wafers from each specimen. Wafers were strategically cut in an effort to maximize opportunities to observe the various hyoid elements, which could not be fully isolated from the soft tissues.

Slide Mounting

Prior to mounting, plastic slides were frosted by grinding them on a Buehler Ecomet4 variable speed grinder wheel (Buehler, Illinois Toolworks, Illinois) to increase the surface area for adherence of the wafer to the slide. Embedded specimen wafers were slide-mounted using Starbond cyanoacrylate instant adhesive (Starbond Premium, California).

Slide Grinding and Polishing

Mounted slides were ground and polished on a Buehler Ecomet4 variable speed grinder wheel, at a speed of 80–120 rotations per minute. As the wafers were ground

down, the grit of the paper was sequentially increased (ground to 2 millimeters using 60 grit paper; 1 mm / 120 grit; 600 μm / 180 grit). Final grinding was performed with a succession of 320, 600, 800, and 1200 grit paper to achieve thin sections of approximately 100–400 μm thick.

Slide Staining Protocol

Following initial histological imaging, I stained all analyzed slides with Toluidine Blue. Materials for the Toluidine Blue staining protocol included 99% Formic Acid (Manofohm: Chemical Supply; Florence, Colorado) that had been diluted to 1% concentration and Toluidine Blue Solution (Sigma-Aldrich, St. Louis). To prime the specimen for Toluidine binding, slides were rocked in formic acid for 30 seconds. The slide was blotted to remove excess formic acid. Prior to staining, the Toluidine Blue Solution was heated for 30 seconds to reach 57° C to stimulate molecular activity. The slides were lowered into the warmed solution for 5 minutes for staining. The slides were then rinsed under running tap water and dried prior to analysis.

Slide Analysis

Slides were visualized using a Nikon digital sight camera and petrographic microscope (DS-U3 and DS-Fi2; Nikon Instruments, New York) and photographed using NIS-Elements: Documentation software (F4.00.00; Nikon Instruments, New York). Specimens were photographed under plane-polarized light. Features of the hyoid apparatus implicating tissue composition, growth, and remodeling were categorized based on observation of each respective specimen.

Results

Osteology

The anole hyoid apparatus is composed of eight unique elements, two of which are unpaired (hyoid body, entoglossal process), six of which are paired (hypohyals, ceratohyals, epihyals, first ceratobranchials, epibranchials, and second ceratobranchials) (Figure 3.1). The entoglossal process projects anteriorly from the hyoid body. The hypohyals project anterolaterally from the hyoid body. Attached to the distal aspect of the hypohyals are the ceratohyals, which project posterolaterally. Attached to the distal aspect of the ceratohyals are the epihyals, which are oriented dorsally. The first ceratobranchials project posterolaterally posterolateral from the posterior border of the hyoid body. Medial to these are the second ceratobranchials, which also project posteriorly from the hyoid body. Attached to the distal aspect of the first ceratobranchials are the epibranchials, which are oriented dorsally.

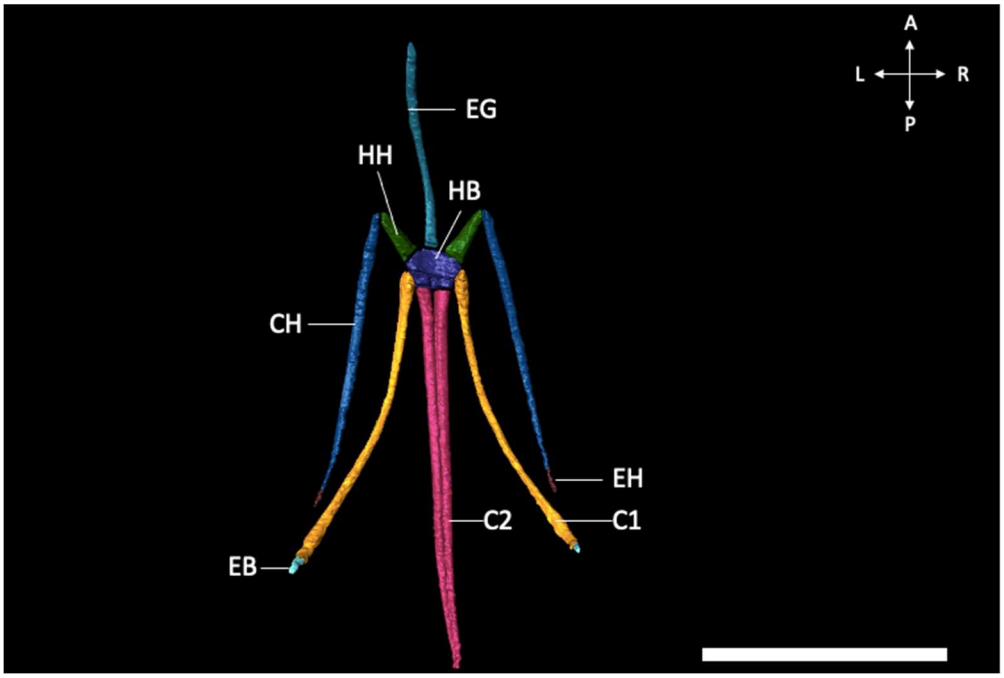

Figure 3.1. *Digitally dissected anole hyoid apparatus.* Gross anatomy of hyoid apparatus in dorsal view as observed using digital dissection (chapter II). This figure will be used as reference for the position of histological slices. Ceratohyal (Dark

Blue; CH), First Ceratobranchial (Orange; C1), Second Ceratobranchial (Magenta; C2), Epibranchial (Light Blue; EB), Entoglossal Process (Turquoise; EG), Epihyal (Brown; EH), Hyoid Body (Purple; HB), Hypohyal (Dark Green; HH). Scale bar = 5 mm. Compass rose orientations: Anterior (A), Posterior (P), Left (L), Right (R).

Histology

Male

Results are described from two slides obtained for male specimens, inclusive of the following sections and orientations: specimen *Anolis* hyoid male 001 is a transverse section that includes the entoglossal process, the hypohyal, and the ceratohyal. Specimen *Anolis* hyoid male 002 provides a second transverse section of the entoglossal process.

- **Anolis *male hyoid 001* (Figure 3.2)**: the elements in this section are observed from their transverse aspect. This section includes the proximal aspect of the entoglossal process, the proximal aspect of each hypohyal, and the proximal aspect of the ceratohyals. The entoglossal process at this position is ovoid in cross section and dorsally compressed. The matrix is cartilaginous (as indicated by violet stain), with visible chondrocytes (blue stain). The edges of the entoglossal process are stained dark purple, indicative of a calcification front. The hypohyals at this position are kidney-bean-shaped in transverse cross section, concave on their dorsal aspect. The matrix is cartilaginous (violet stain). The edges of the hypohyals are stained dark purple, indicative of a calcification front. The edges of the hypohyals show evidence of osteoclast reworking, particularly along their lateral aspects. The ceratohyals at this position are ovoid in cross section, and dorsally compressed. The ceratohyal matrix is cartilaginous (violet stain). The edges of the ceratohyals are dark purple, indicative of a calcification front (black arrows in Figure 3.2).

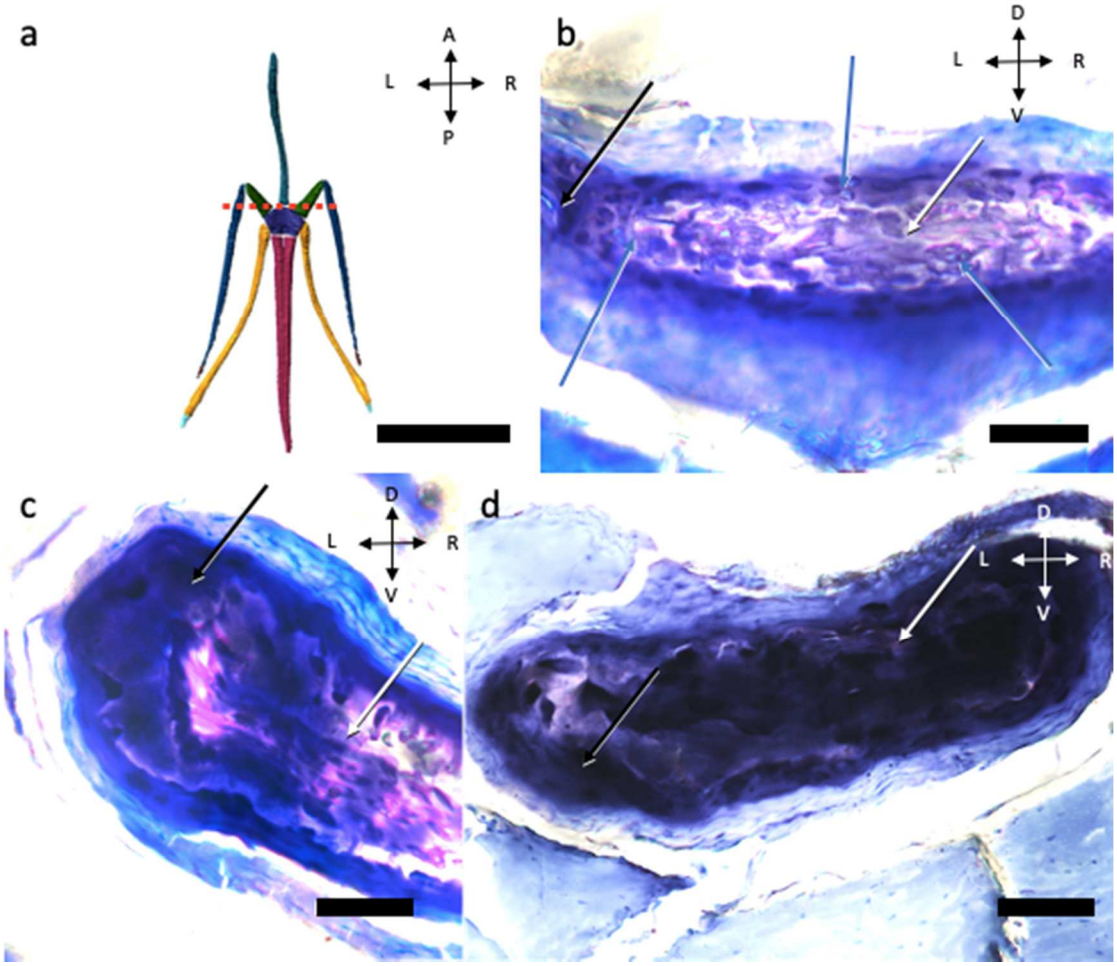

Figure 3.2. *Anolis male hyoid 001*. Histology of hyoid apparatus from *Anolis* male hyoid 001. a. Relative position of slice in hyoid apparatus, indicated by red dashed line; scale bar = 5 mm b. Entoglossal process; scale bar = 100 µm. c. Hypohyal; scale bar = 100 µm. d. Ceratohyal; scale bar = 100 µm. White arrows indicate cartilaginous matrix. Light blue arrows indicate chondrocytes. Black arrows indicate calcification front. All images are 20x magnification. Compass rose orientations: Anterior (A), Posterior (P), Left (L), Right (R), Dorsal (D), Ventral (V).

- **Anolis *male hyoid 002* (Figure 3.3):** the elements in this section are observed in the transverse plane. The section includes the entoglossal process (Figure 3.3). At this position, the entoglossal process is circular in cross section and its matrix is cartilaginous (violet). Paired isogenous groups of chondrocytes (blue) are observable along the edges of the structure, particularly its ventral aspect.

Sharpey's fiber-like anchors are observable, particularly along the dorsal aspect, at the insertion point of *M. verticalis* muscle.

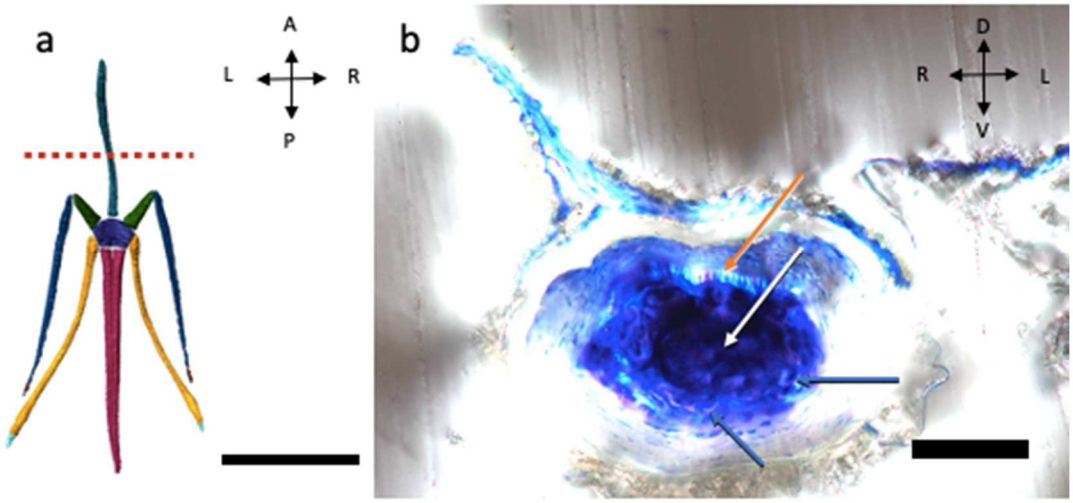

Figure 3.3 *Anolis male hyoid 002.* Histology of hyoid apparatus from *Anolis* male hyoid 002. a. Relative position of slice in hyoid apparatus indicated by red dashed line. Scale bar = 5 mm b. Entoglossal process; Scale bar = 100 µm. White arrow indicates cartilaginous matrix. Blue arrows indicate chondrocytes. Orange arrow indicates Sharpey's fiber like bundles. Image is 20x magnification. Compass rose orientations: Anterior (A), Posterior (P), Left (L), Right (R), Dorsal (D), Ventral (V).

Female

Results are described for two slides obtained for female specimens, inclusive of the following sections and orientations: specimen *Anolis* female hyoid 001 is a transverse section that includes a transverse section the second ceratobranchials, and specimen *Anolis* female head 001 is transverse section that includes a transverse section of the ceratohyals, a transverse section of the first ceratobranchials, and a transverse section of the second ceratobranchials.

- **Anolis *female hyoid 001* (Figure 3.4)**: the elements in this section are observed from their transverse aspect. This section includes the proximal aspect of one of the second ceratobranchials (Figure 3.4b). At this position, the second ceratobranchials are kidney bean shaped in cross section, convex along their

dorsal aspect. The core is mineralized with cartilage islands. No well-defined perichondrium is observed.

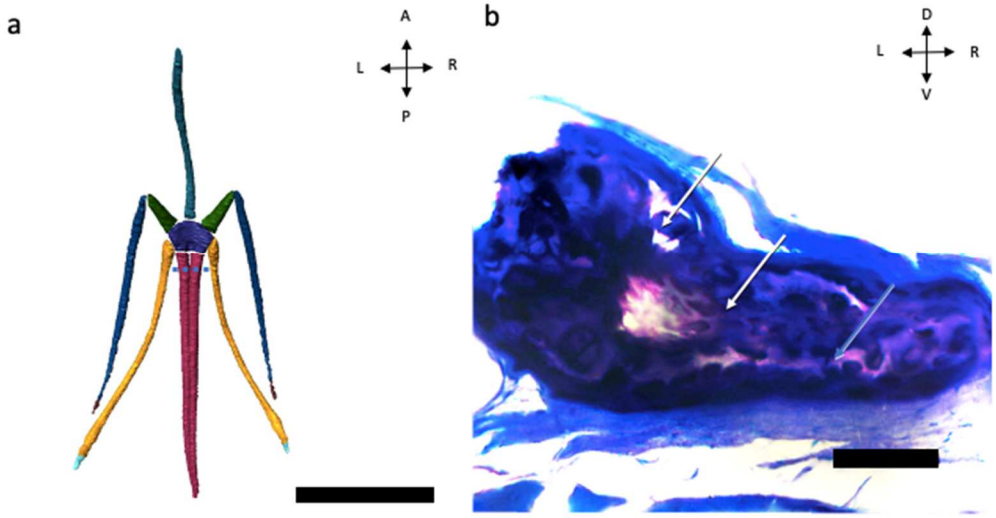

Figure 3.4. *Anolis female hyoid 001* Histology of hyoid apparatus from *Anolis* female hyoid 001. a. relative position of slice in hyoid apparatus, indicated by blue dashed line; scale bar = 5 mm. b. second ceratobranchial; scale bar = 100 µm. White arrows indicate cartilage islands. Light blue arrow indicates chondrocytes. White scale bar = 5 mm. Black scale bar = 100 µm Image is 20x magnification. Compass rose orientations: Anterior (A), Posterior (P), Left (L), Right (R), Dorsal (D), Ventral (V).

- **Anolis *female head 001* (Figure 3.5):** the elements in this section are observed from their transverse aspect. This section included the ceratohyals, the first ceratobranchials, and the second ceratobranchials. At this position, the ceratohyals are ovoid in cross section and dorsoventrally compressed (Figure 3.5b). The ceratohyal matrix is cartilaginous (violet). The edge of the ceratohyal is dark purple, indicative of a calcification front.

  The first ceratobranchial at this position is ovoid and dorsoventrally compressed (Figure 3.5c). The edges of the first ceratobranchial are jagged and scalloped in texture. Staining light purple (indicating osteoid), it is compositionally distinct from the other bones of the specimen, with distinctive osteocytes present. The first ceratobranchial has a hollow core. The second

ceratobranchial at this position is roughly club shaped in cross section (Figure 3.5d). The second ceratobranchial is scalloped along its dorsal and lateral aspects. The matrix of the second ceratobranchial is cartilaginous (violet).

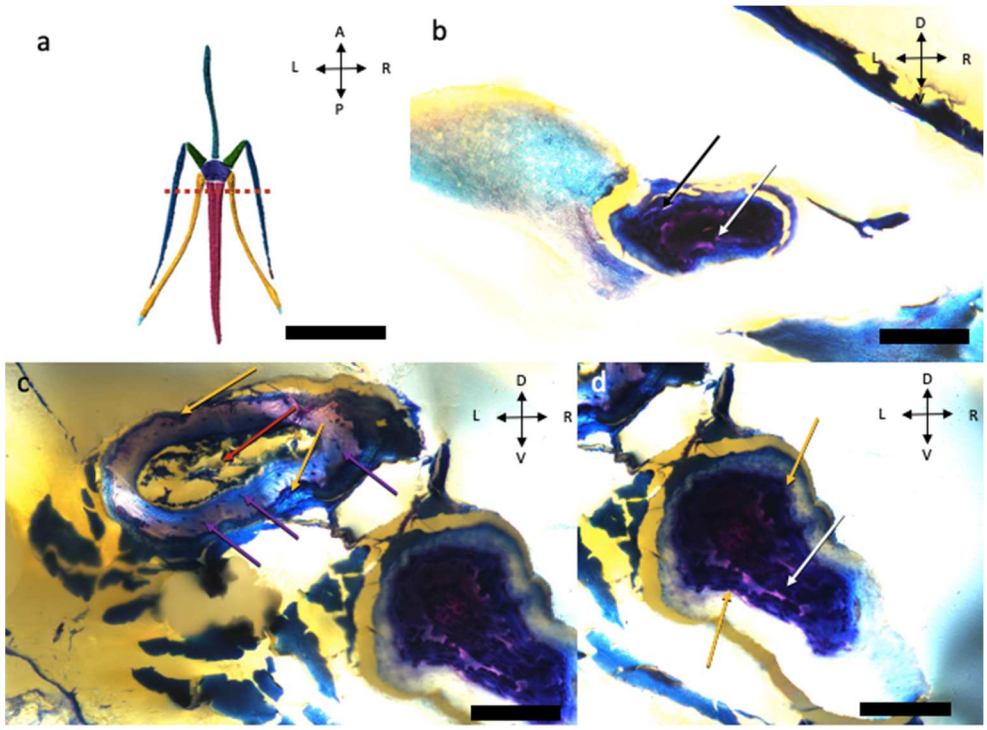

Figure 3.5. *Anolis female head 001.* Histology of hyoid apparatus from *Anolis* female head 001. a. Relative position of slice in hyoid apparatus, indicated by red dashed line; scale bar = 5 mm. b. Ceratohyal; scale bar = 100 µm. c. First Ceratobranchial; 100 µm. D. Second ceratobranchial; 100 µm. White arrows indicate cartilage. Black arrows indicate calcification fronts. Gold arrows indicate scalloped edges. Red arrow indicates hollow core. Purple arrow indicates osteocyte lacunae. All images magnified 20x. Compass rose orientations: Anterior (A), Posterior (P), Left (L), Right (R), Dorsal (D), Ventral (V).

Putative Juvenile

Results are described for one slide obtained for putative juvenile specimens, inclusive of the following sections and orientations: specimen *Anolis* juvenile hyoid 001 is a transverse section including the hyoid body and the ceratohyals.

- ***Anolis* juvenile hyoid 001 (Figure 3.6):** the elements in this section were observed from their transverse aspect. This section included the ceratohyals and

the hyoid body (Figure 3.6). The ceratohyals are embedded with fibroblasts (note the large, elongate, flattened shape, with extended processes along the ends of the cell bodies; Figure 3.6b) and have jagged, scalloped edges. The hyoid body has an observable perichondrium (Figure 3.6c; Figure 3.6d). The structure's matrix is embedded with fibroblasts and chondrocytes. Observable islands of cartilaginous matrix are present that are surrounded by fibroblasts.

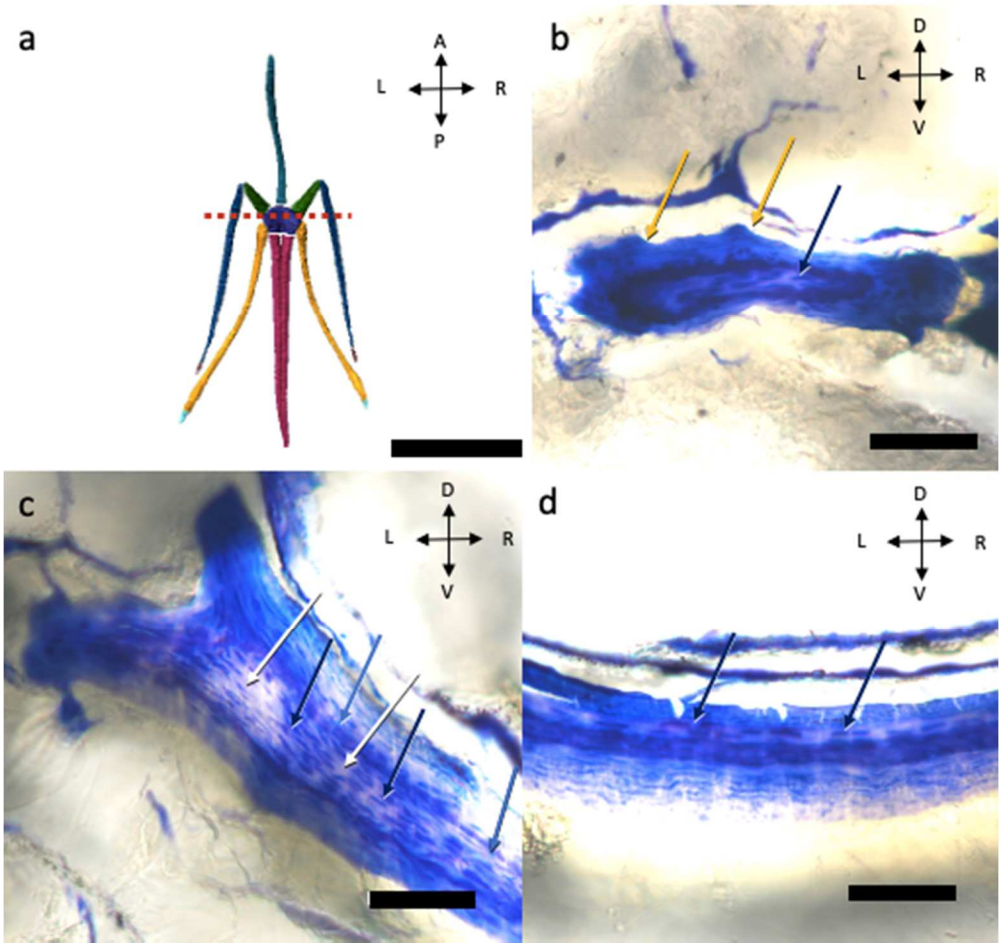

Figure 3.6. *Anolis juvenile hyoid 001.* Histology of hyoid apparatus from *Anolis* juvenile hyoid 001. a. Relative position of slice in hyoid apparatus, indicated by red dashed line; scale bar = 5 mm. b. Ceratohyal; scale bar = 100 µm. c. Hyoid body, lateral aspect; scale bar = 100 µm. d. Hyoid body, medial aspect; scale bar = 100 µm. Dark Blue arrows indicate fibroblasts. White arrows indicate cartilage islands. Gold arrows indicate scalloped edges. White scale bar = 5mm. Black scale bar = 100µm. All images magnified 20x. Compass rose orientations: Anterior (A), Posterior (P), Left (L), Right (R), Dorsal (D), Ventral (V).

Discussion

In the putative mature specimens, the hypohyals, ceratohyals, and second ceratobranchials were observed to be primarily cartilaginous in the sections obtained. This agrees with the observations of the structure by Bels (1990) and Font and Rome (1990). Corroborating Bels (1990), who also worked with *A. carolinensis*, these elements all had observable chondrocytes, with specimens consistently displaying chondrocytes in paired isogenous groups (Figure. 3.2b; 3.3b). This consistency is noteworthy, as *A. carolinensis* is much smaller morphologically than *A. equestris*. The respective hyoid apparatus is also much smaller in *A. carolinensis*, meaning isogenous group patterning could potentially be related to the size of the cartilaginous structure. A distinctive condition was observed in the first ceratobranchial of the mature female, wherein the structure was composed of bone with distinct osteocytes (Figure 3.5c). This structure was also distinctive by the presence of an apparent lumen hollowing out the matrix of the element at the position of the slice, a characteristic that was not observed in either of the previous studies.

While the adult specimens generally followed the results of previous studies on the anole hyoid histology (with the aforementioned exceptions), unique observations were made regarding the putative juvenile specimen. The observed hyoid body in the juvenile specimen (Figure 3.6c; 3.6d) structurally appears to be cartilaginous (with discernible chondrocytes), and has observable fibroblasts, multipotent cells that can form cartilaginous structures (Sorrell and Caplan, 2009). It is possible that this structure is in fact composed of fibrocartilage, which is in contrast with the elements observed in the adult male and female, which had chondrocytes or osteocytes embedded in their matrix. Without 1:1 comparisons of the hyoid bodies across ontogeny, it is difficult to draw

concrete conclusions on the implications of these discrepancies in tissue composition. The juvenile hyoid body, however, does present what appears to be an anlage (Hashi et al, 2009), a rudimentary basis of the hyoid structure which has now incorporated into the mature hyoid body. This pattern of growth has been observed in fibrocartilage structures, such as the intervertebral discs (Rufai et al, 1995).

Histologically, it appears that minimal dimorphism exists between the hyoid apparatuses of male and female anoles (Figure 3.2; Figure 3.3; Figure 3.4; Figure 3.5). Both are cartilaginous with observable osteocytes or chondrocytes embedded in their matrices. However, all these structures display jagged edges. This is an interesting observation with the potential fibrocartilage basis observed in the juvenile hyoid, as this pattern is consistent with the appearance of mineralization of fibrocartilage (Walters et al, 2019). This analysis potentially represents the first description of fibrocytes in the anole hyoid apparatus. Without precise age of the specimen, it is difficult to discern when this developmental shift occurs in *Anolis*.

While not the primary aim of this analysis (which was to observe for structural indicators of muscular attachment), many of the hyoid bones retained muscular attachments. One structure (male entoglossal process) had observable fibers that in appearance were comparable to Sharpey's fibers. However, for most bones the musculature appeared to be simply adhered to the structure, which is an interesting method of attachment due to even ossified bones having fibrocartilage at muscular attachment sites (Lu et al, 2008).

Evolutionarily, these observations provide a unique lens of the anole dewlap. While the male *A. carolinensis* hyoid apparatus is both morphologically larger, and the males

behaviorally open the dewlap more frequently than females, this appears to have no impact in the histology of the structures. With this, the interaction directly at the interface of the cartilage and musculature in the complex, jointed system of the anole hyoid apparatus is noteworthy, possibly indicative of the relationship between muscles and cartilaginous bone for complex actions. These interactions are not observable in most tetrapods, or even animals with specialized cartilaginous skeletons such as sharks (Seidel et al, 2020).

Future Directions

There are many future directions from this analysis, some addressing weaknesses in the current study, others are novel and based on the findings discussed above. Firstly, while sexually dimorphic variation is not apparent, variation in hyoid histology could be apparent in taxa with and without dewlap structures. This makes the Iguania an excellent model group for an analysis of how novel, complex functions of gross anatomical structures impact the underlying histology. This system is particularly apropos because convergent hyoid specializations appear repeatedly within some members of this group whereas others maintain unique hyoid phenotypes (Ord et al, 2015). Histological comparison should also be done between Iguania and other groups of squamates, to observe if any unique, histologically identifiable characters are present in the Iguania.

A limitation of the present study was the inability to precisely age the observed specimens, limiting interpretations of shifts in growth pattern and structural composition. Future research should observe anole hyoid development as a well-documented ontogenetic series, allowing precise calibrations of shifts in growth pattern and composition to specific life stages. This could be further improved with analysis of

ontogenetic series for each sex as well and 1:1 comparisons of all hyoid elements across male, female, and putative juvenile specimens. The lack of strictly targeted histological sectioning in the current study is an artifact of the exploratory nature of this work and the explicit goal of establishing the best protocols for histologically observing the anole hyoid apparatus. In addition, this strict targeting should also aim for analysis of the joints in the hyoid structure to directly observe the interactions of the elements and associated joint tissues at the microanatomical level. The hyoid apparatuses of anoles should also be compared directly to other tetrapod hyoids (both with and without growth series), to compare their growth pattern in primarily cartilaginous hyoids to primarily ossified hyoids (Li et al, 2018; Hartl et al, 2021; Shimizu et al, 2005). Further, the additional use of other staining protocols should be applied to the anole hyoid as well. On a larger scale, with the inconsistent mineralization pattern of the hyoid elements, the anole hyoid apparatus presents a unique model to observe the mechanisms by which cartilage calcifies non-pathologically.

The combination of these future directions, along with the observations of this study, will continue to expand upon the ability to use *Anolis* as a deep time evolutionary model. Their distinctive hyoids (both morphologically and functionally), along with the robust background of ecological research on the genus (Nicholson et al, 2007; Vanhooydonck et al, 2005; Vanhooydonck et al, 2009), make *Anolis* an excellent model for understanding functional implications of unique structures. Future work should continue on the anole hyoid apparatus as well as structures like it, to further integrate histological observation into the morphology, performance, fitness paradigm in research on both extant and deep time models.

REFERENCES

Adams, A., Mankad, K., Offiah, C., Childs, L. (2016) Branchial Cleft Anomalies: A Pictorial Review of Embryological Development and Spectrum of Imaging Findings. *Insights Imaging 7*, 69-76. https://doi.org/10.1007/s13244-015-0454-5

Ahlberg, P. E. (2019). Follow the Footprints and Mind the Gaps: A New Look at the Origin of Tetrapods. *Earth and Environmental Science Transactions of the Royal Society of Edinburgh 109*, 115-137. https://doi.org/10.1017/S1755691018000695

Amiel, D., Frank, C., Harwood F., Fronek J., Akeson, W. (1984). Tendons and Ligaments: A Morphological and Biochemical Comparison. *Journal of Orthopaedic Research 1*, 257-265. https://doi.org/10.1002/jor.1100010305

Anderson, P. S. L., Westneat, M. W. (2007). Feeding Mechanics and Bite Force Modelling of the Skull of *Dunkleosteus terrelli*, an Ancient Apex Predator. *Biology Letters 3*, 76-79. https://doi.org/10.1098/rsbl.2006.0569

Apostolakos, J., Durant, T. J. S., Dwyer C. R., Russell, R. P., Weinreb, J. H., Alaee, J. H., Beitzel, K., McCarthy, M. B., Mazzocca, A. D. (2014). The Enthesis: A Review of the Tendon-to-Bone Insertion. *Muscles, Ligaments, and Tendons Journal 4(3)*, 333-342.

Arnold, S. J. (1983). Morphology, Performance, Fitness. *American Zoologist 23*(2), 347-361. https://doi.org/10.1093/icb/23.2.347

Arokoski, J. P. A., Jurvelin, J. S., Väätäinen, U., Helminen, H. J. (2000). Normal and Pathological Adaptations of Articular Cartilage to Joint Loading. *Scandinavian Journal of Medicine and Science in Sports 10*, 186-198. https://doi.org/10.1034/j.1600-0838.2000.010004186.x

Auvenshine, R. C., Pettit, N. J. (2018). The Hyoid Bone: An Overview. *The Journal of Craniomandibular Sleep Practice 38*(1), 6-14. https://doi.org/10.1080/08869634.2018.1487501

Barmakian, J. T. (1992). Anatomy of the Joints of the Thumb. *Hand Clinics 8(4)*, 683-691. https://doi.org/10.1016/S0749-0712(21)00735-6

Baber, E. C. (1855). On the Structure of Hyaline Cartilage. *Journal of Anatomy and Physiology 10*, 111-126.

Bell T. (1826). Observations sur la Structure du Gosier du Genra *Anolis*. *Ann Sci Nat 7*, 191-195.

Bellairs, A. (1970) The Life of Reptiles. New York: Universe Books.

Bels. V. L., (1990). The Mechanism of Dewlap Extension in *Anolis carolinensis* (Reptilia: Iguanidae) with Histological Analysis of the Hyoid Apparatus. *Journal of Morphology 206*, 225-244. https://doi.org/10.1002/jmor.1052060209

Benjamin, M., Evans, E. J. (1990). Fibrocartilage. *Journal of Anatomy 171*, 1-15.

Benjamin, M., Kumai, T., Milz, S., Boszczyk, B. M., Bosczyk, A. A., Ralphs, J. R. (2002). The Skeletal Attachment of Tendons – Tendon Entheses. *Comparative Biochemistry and Physiology Part A 133*, 931-945.

Bicknell, R. D. C., Klinkhamer, A. J., Flavel R. J., Wroe, S. Paterson J. R. (2018). A 3D Anatomical Atlas of Appendage Musculature in the Chelicerate Arthropod *Limulus polyphemus*. *PLoS ONE 13*(2), e0191400. https://doi.org/10.1371/journal.pone.0191400

Biewener, A. A. (1991). Musculoskeletal Design in Relationship to Body Size. *Journal of Biomechanics 24*, 19-29. https://doi.org/10.1016/0021-9290(91)90374-v

Biewener, A., Alexander, R. M., Heglund, N. C. (1981). Elastic energy storage in the hopping of kangaroo rats (*Dipodomys spectablis*). *Journal of Zoology 195*, 369-383. https://doi.org/10.1111/j.1469-7998.1981.tb03471.x

Blair, H. C., Kahn, A. J., Crouch, E.C., Jeffrey, J. J., Teitelbaum, S. L. (1986). Isolated Osteoclasts Resorb the Organic and Inorganic Components of Bone. *The Journal of Cell Biology 102*, 1164-1172. https://doi.org/10.1083/jcb.102.4.1164

Borg, E., Zakrisson, J. E. (1975). The Activity of the Stapedius Muscle in Man During Vocalization. *Acta Oto-Laryngologica 79*, 325-333. https://doi.org/10.3109/00016487509124694

Brainerd, E. L., Baier, D. B., Gatesy, S. M., Hedrick T. L., Metzger, K. A., Gilbert, S. L., Crisco, J. L. (2010). X-Ray Reconstruction of Moving Morphology (XROMM): Precision, Accuracy and Applications in Comparative Biomechanics Research. *Journal of Experimental Zoology 313A*, 262-279. https://doi.org/10.1002/jez.589

Brenna C. T. A. (2021). Bygone Theatres of Events: A History of Human Anatomy and Dissection. *The Anatomical Record 305*, 788-802. https://doi.org/10.1002/ar.24764

Briggs, D. E. G., Wilby, P. R., Pérez-Moreno, B. P., Sanz J. L., and Fregenal-Martinez M. (1997). The Mineralization of Dinosaur Soft Tissue in the Lower Cretaceous of Las Hoyas, Spain. *Journal of the Geological Society 154*, 587-588.

Bruckner, P., van der Rest, M. (1994). Structure and Function of Cartilage Collagens. *Microscopy Research and Techniques 28*, 378-384.

Burrows, A. M., Waller, B. M., Parr, L. A., Bonar, C. J. (2006). Muscles of Facial Expression in the Chimpanzee (*Pan troglodytes*): Descriptive, Comparative, and Phylogenetic Contexts. *Journal of Anatomy 208*, 153-167. https://doi.org/10.1144/gsjgs.154.4.0587

Camilieri-Asch V., Show, J. A., Mehnert, A., Yopack, K. E., Partridge, J. C., Collin, S. P. (2020). diceCT: A Valuable Technique to Study the Nervous System of fish. *Evolutionary Neurology 7(4)*, 1-23. https://doi.org/10.1523/ENEURO.007620.2020

Cammarata, M. L., Dhaher, Y. Y. (2012). Associations Between Frontal Plane Joint Stiffness and Proprioceptive Acuity in Knee Osteoarthritis. *Arthritis Care and Research 64(5)*, 35-743. https://doi.org/10.1002%2Facr.21589

Cox, P. G., Faulkes, C. G. (2014) Digital Dissection of the Masticatory Muscles of the Naked Mole-Rat *Heterocephalus glaber* (Mammalia, Rodentia). *PeerJ 2*(1), e44. https://doi.org/10.7717/peerj.448

Cox, R. W., Peacock, M. A., (1977). The Fine Structure of Developing Elastic Cartilage. *Journal of Anatomy 123(2)*, 283-296.

Crane, J. F., Trainor, P. A. (2006). Neural Crest Stem and Progenitor Cells. *Annual Review of Cell and Developmental Biology 22*, 267-86. https://doi.org/10.1146/annurev.cellbio.22.010305.103814

Dahl, T. W., Hammarlund, E. U., Anbar, A. D., Bond D. P. G., Gill, B. C., Gordon, G. W., Knoll A. H., Nielsen, A. T., Schovsbo, N. H., Canfield, D. E. (2010). Devonian Rise in Atmospheric Oxygen Correlated to the Radiations of Terrestrial Plants and Large Predatory Fish. *PNAS 107*(42), 17911-17915. https://doi.org/10.1073/pnas.1011287107

Dearden, R. P., Stockey, C., Brazeau, M. D. (2019). The Pharynx of the Stem-Chondrichthyan *Ptomacanthus* and the Early Evolution of the Gnathostome Gill Skeleton. *Nature Communications 10*, 2050. https://doi.org/10.1038/s41467-019-10032-3

Dubois, P. (2014). The Skeleton of Postmetamorphic Echinoderms in a Changing World. *Biological Bulletin 226*, 223-236. https://doi.org/10.1086/BBLv226n3p223

Echelle, A. F., Echelle, A. A., Fitch, H. S. (1978). Inter- and Intraspecific Allometry in a Display Organ: The Dewlap of *Anolis* (Iguanidae) Species. *Copeia 2*, 245-250.

Edgeworth, F. H. (1935). The Cranial Muscles of Vertebrates. Cambridge University Press. https://doi.org/10.2307/1443558

Elias-Costas, A. J., Montesinos, R., Grant, T., Faivovich J. (2017). The Vocal Sac of Hylodidae (Amphibia, Anura): Phylogenetic and Functional Implications of Unique Morphology. *Journal of Morphology 278*(11), 1506-1516. https://doi.org/10.1002/jmor.20727

Erickson, G. M., Gignac, P. M., Steppan, S. J., Lappin, A. K., Vliet, K. A., Brueggen, J. D., Inouye, B. D., Kledzik, D., Webb, G. J. W. (2012). Insights into the Ecology and Evolutionary Success of Crocodilians Revealed through Bite-Force and Tooth Pressure Experimentation. *PLoS One 7*(3), e31781. https://doi.org/10.1371/journal.pone.0031781

Evans, D.H., Piermarini, P. M., Choe K. P. (2005). The Multifunctional Fish Gill: Dominant Site of Gas Exchange. Osmoregulation, Acid-Base Regulation, and Excretion of Nitrogenous Waste. *Physiological Review 85*, 98-177. https://doi.org/10.1152/physrev.00050.2003

Feng, X., Teitelbaum, S. L. (2013). Osteoclasts: New Insights. *Bone Research 1*, 11-26. https://doi.org/10.4248/br201301003

Fenwick, S. A., Gregg, P. J., Rooney, P. (1999). Osteoarthritic Cartilage Loses its Ability to Remain Avascular. *Osteoarthritis and Cartilage 7*, 441-452. https://doi.org/10.1053/joca.1998.0238

Field, D. J., Lin, S. C., Ben-Zvi, M., Goldbogen, J. A., Shadwick, R. E. (2011). Convergent Evolution Driven by Similar Feedings Mechanics in Balaenopterid Whales and Pelicans. *The Anatomical Record 294*. 1273-1282. https://doi.org/10.1002/ar.21406

Filipowska, J., Tomaszewki, K. A., Niedźwiedzki, L., Walocha, J. A., Niedźwiedzki, T. (2017). The role of vasculature in bone development, regeneration, and proper systemic functioning. *Angiogenesis 20*, 291-302. https://doi.org/10.1007%2Fs10456-017-9541-1

Fiorelli, L. E., Ezcurra M. D., Hechenleitner E. M., Argañararaz, Taborda, J. R. A., Trotteyn M. J., von Baczko M. B., Desoja J. B. (2013). The Oldest Known Known Communal Latrines Provide Evidence of Gregarism in Triassic Megaherbivores. *Scientific Reports 3*, 3348. https://doi.org/10.1038/srep03348

Font, E., Rome L. C. (1990). Functional Morphology of Dewlap Extension in the Lizard *Anolis equestris* (Iguanidae). *Journal of Morphology 206*, 245-258. https://doi.org/10.1002/jmor.1052060210

Fornalski S., Gupta R., and Lee T. Q. (2003). Anatomy of Biomechanics of the Elbow Joint. *Sports Medicine and Arthroscopy Review 11*, 1-9. https://doi.org/10.1097/00130911-200312000-00008

Fuss, F. K. (1991) The Ulnar Collateral Ligament of the Human Elbow Joint. Anatomy, Function, and Biomechanics. *Journal of Anatomy 175*, 203-212.

Gamble, T., Bauer, A. M., Greenbaum, E., Jackman, T. R. (2008). Out of the Blue: A Novel, Trans-Atlantic Clade of Geckos. *Zoologica Scripta 37(4)*, 355-366. https://doi.org/10.1643/OT-13-166

Geissmann, T., (2000). Duet Songs of the Siamang, *Hylobates syndactylus*: I Structure and Organization. *Primate Reports 56*, 33-60.

Gemeno, A. I. C., Orozco, J. R. W., Nogues, J. A., Gotor, C. Y., de la Torre, M. A. C., Orozco, A. W. (2009) Contribution to Morphological Knowledge of the Developing Human Incudo-Mallear Joint. *Acta Oto-Laryngologica 129*, 1380-1387. https://doi.org/10.3109/00016480902849435

Gignac P. M., Kley N. J. (2014). Iodine-Enhanced Micro-CT Imaging: Methodological Refinements for the Study of the Soft-Tissue Anatomy of Post-Embryonic Vertebrates. *Journal of Experimental Biology 332B*, 166-176. https://doi.org/10.1002/jez.b.22561

Gignac, P., Kley, N. J., Clarke, J. A., Clarke, Colbert, M. W., Morhardt, A. C., Cerio, D., Cost, I. N., Cox, P. G., Daza, J. D., Early, C. M., Echols, M. S., Henkelman, R. M., Herdina, A. N., Holliday, C. M., Li, Z., Mahlow, K., Merchant S., Müller, J., Orsbon, C. P., Paluh, D. J., Thies, M. L., Tsai, Witmer, L. M. (2016). Diffusible Iodine-Based Contrast-Enhanced Computed Tomography (diceCT): an Emerging Tool for Rapid, High-Resolution, 3-D Imaging of Metazoan Soft Tissues. *Journal of Anatomy 228*, 889-909. https://doi.org/10.1111/joa.12449

Gignac, P., O'Brien, H. Suchian Feeding Success at the Interface of Ontogeny and Macroevolution. *Integrative and Comparative Biology 56*(3), 449-458. https://doi.org/10.1093/icb/icw041

Gnanamuthu, C. P. (1937). Comparative Study of the Hyoid and Tongue of Some Typical Genera of Reptiles. *Proceedings of the Zoological Society of London B 16*, 1-66. https://doi.org/10.1111/j.1096-3642.1937.tb00821.x

Goodman, R. M. (2010). Evidence of Divergent Growth Rates Among Populations of the Lizard *Anolis carolinensis* based on experimental manipulations of egg size. *Population Ecology 52*, 113-122. http://dx.doi.org/10.1007/s10144-009-0167-z

Graham J., Richardson, J. (2012). Developmental and Evolutionary Origins of the Pharyngeal Apparatus. *EvoDevo 3*(24). https://doi.org/10.1002%2Fwdev.147

Green, E. J., MaRae, L., Freeman R., Harfoot M. B. J., Hill S. L. L., Baldwin-Cantello, W., Simonson, W. D. (2020). Below the Canopy: Global Trends in Forest Vertebrate Populations and their Drivers. *Proceedings Royal Society B 287*, 20200553. https://doi.org/10.1098/rspb.2020.0533

Gu, Y., Sorokin, L., Durbeej, M., Hjalt, T., Jonsson, J., Ekblom, M. (1999). Characterization of Bone Marrow Laminins and Identification of α5-Containing Laminins as Adhesive Proteins for Multipotent Hematopoietic FDCP-Mix Cells. *Blood 93(8)*, 2533-2542.

Hall B. K. (2008). The Neural Crest and Neural Crest Cells: Discovery and Significance for Theories of Embryonic Organization. *Journal of Bioscience 33*(5), 781-793. https://doi.org/10.1007/s12038-008-0098-4

Hannam A. G., McMillan, A. S. (1994) Internal Organization in the Human Jaw Muscles. *Critical Reviews in Oral Biology Medicine 5*(1), 55-89. https://doi.org/10.1177%2F10454411940050010301

Hartl, B., Egerbacher, M., Kneissl, S. M. (2021). Correlated Imaging of the Equine Hyoid Apparatus Using CT, Micro-CT, and Histology. *Frontiers in Veterinary Science 8*, 652563. https://doi.org/10.3389/fvets.2021.652563

Hashi, H., Yoshida, H., Honda, K., Fraser, S., Kubo, H., Awane, M., Takabayashi, A., Nakano, H., Yamaoka, Y., Nishikawa, S. (2001). Compartmentalization of Peyer's Patch Anlagen Before Lymphocyte Entry. *Journal of Immunology 166*, 3702-3709. https://doi.org/10.4049/jimmunol.166.6.3702

Herrel A., Meyers, J. J., Aerts, P, Nishikawa K. C. (2001). Functional Implications of Supercontracting Muscle in the Chameleon Tongue Retractors. *The Journal of Experimental Biology 204*, 3621-3627. https://doi.org/10.1242/jeb.204.21.3621

Hiiemae, K. M., Palmer J. B. (2003). Tongue Movements in Feeding and Speech. *Critical Reviews in Oral Biology Medicine 14*(6), 413-429. https://doi.org/10.1177/154411130301400604

Hirasawa, T., Kuratani, S. (2015). Evolution of the Vertebrate Skeleton: Morphology, Embryology, and Development. *Zoological Letters 1(2)*, 1-17.

Hoggan, G., Hoggan, F. E. (1880). On the Lymphatics of Cartilage or of the Perichondrium. *Journal of Anatomy and Physiology 15*, 120-136.

Holland, Z. H. (2002). Heads or Tails? Amphioxus and the Evolution of Anterior-Posterior Patterning in Deuterostomes. *Developmental Biology 241*, 209-228. https://doi.org/10.1006/dbio.2001.0503

Jaffar, A. A., Abass, S. J., Ismael, M. Q. (2006). Biomechanical Aspects of Shoulder and Hip Articulations: A Comparison of Two Ball and Socket Joints. *Al-Khwarizmi Engineering Journal 2(1)*, 1-14.

Janvier, P. (1999) Catching the First Fish. *Nature 402*, 21-22.

Jenssen, T.A. (1978) Display diversity in anoline lizards and problems of interpretation. In N. Greenberg and P.D. MacLean**(eds):** Behavior and Neurology of Lizards. Rock-**ville:** National Institute

Jones, M. E. H., Curtis, N., O'Higgins, P., Fagan, M., Evans, S. E. (2009). The Head and Neck Muscles Associated with Feeding in *Sphenodon* (Reptilia: Lepidosauria: Rhynchocephalia). *Paleontologica Electronica 12(2)*, 56p.

Kardong K.V. (2011). Vertebrates: Comparative Anatomy, Function, Evolution. Sixth Edition. McGraw-Hill Education.

Kawashima, T., Thorington, R. W., Bohaska, P. W., Sato, F. (2017). Evolutionary Transformation of the Palmaris Longus Muscle in Flying Squirrels (Pteromyini: Sciuridae): An Anatomical Consideration of the Origin of the Uniquely Specialized styliform Cartilage. *The Anatomical Record 300*, 340-352. https://doi.org/10.1002/ar.23471

Khan, I. M., Redman, S. N., Williams, R., Dowthwaite, G. P., Oldfield, S. F., Archer, C. W. (2007). The Development of Synovial Joints. *Current Topics in Developmental Biology 79*, 1-36. http://dx.doi.org/10.1016/S00702153(06)79001-9

Kheir, E., Shaw, D. (2009) Hyaline Articular Cartilage. *Orthopaedics and Trauma 23(6)*, 450-455. https://doi.org/10.1016/j.mporth.2009.01.003

Klug C., Frey L., Korn D., Jattiot R., Rücklin M. (2016). The Oldest Gondwanan Cephalopod Mandibles (Hangenberg Black Shale, Late Devonian) and the Mid-Paleozoic Rise of Jaws. *Palaeontology 59*(5), 611-629. https://doi.org/10.1111/pala.12248

Klug, C. De Baets, K., Kröger, B., Bell, M. A., Korn, D., Payne, J. L. (2014). Normal Giants? Temporal and Latitudinal Shifts of Paleozoic Marine Invertebrate Gigantism and Global Change. *Lethaia 48*(2), 267-288. http://dx.doi.org/10.1111/let.12104

Koolsta J. H. and van Eijden (2005). Combined Finite-Element and Rigid-Body Analysis of Human Jaw Joint Dynamics. *Journal of Biomechanics 38*, 2431-2439. https://doi.org/10.1016/j.jbiomech.2004.10.014

Kraus, K. H. (2006). Mesenchymal Stem Cells and Bone Regeneration. *Veterinary Surgery 35*, 232-242. https://doi.org/10.1111/j.1532-950x.2006.00142.x

Kusakabe, R., Kuratani, S. (2007). Evolutionary Perspective from Development of Mesodermal Components in the Lamprey. *Development Dynamics 236*, 2410-2420. https://doi.org/10.1002/dvdy.21177

Lailvaux, S. P., Gilbert, R. L., Edwards, J. R. (2012). A performance-based cost to honest signaling in male green anole lizards (*Anolis carolinensis*). *Proceedings of the Royal Society B 279*, 2841-2848. http://dx.doi.org/10.1098/rspb.2011.2577

Lamoureux, F., Baud'huin, M., Duplomb, L., Heymann, D., Rédini, F. (2007). Proteoglycans: Key Partners in Bone Cell Biology. *BioEssays 29*, 758-771. Langerhans R. B., Knouft J. H., Losos J. B. (2007). Shared and Unique Features of Diversification in Greater Antillean *Anolis* Ecomorphs. *Evolution*. *60*(2), 362-369. https://doi.org/10.1002/bies.20612

Lauder, G. V., Shaffer, H. B. (1988). Ontogeny of Functional Design in Tiger Salamanders (*Ambystoma tigrinum*): Are Motor Patterns Conserved During Major Morphological Transformations. *Journal of Morphology 197*, 249-268. https://doi.org/10.1002/jmor.1051970302

Lautenschlager, S., Bright, J. A., Rayfield, E. J. (2014). Digital Dissection – Using Contrast-Enhanced Computed Tomography Scanning to Elucidate Hard- and Soft-Tissue Anatomy in the Common Buzzard *Buteo buteo*. *Journal of Anatomy 224*, 412-431. https://doi.org/10.1111/joa.12153

Lenfant, C., Johansen, K. (1972). Gas Exchange in Gill, Skin, and Lung Breathing. *Respiration Physiology. 14*, 211-218. https://doi.org/10.1016/00345687(72)90029-1

Li Z., Zhou Z., Clarke, J. A. (2018). Convergent Evolution of a Mobile Bony Tongue in Flighted Dinosaurs and Pterosaurs. *PLoS ONE 13*(6), E0198078. https://doi.org/10.1371%2Fjournal.pone.0198078

Lovern, M. B., Holmes, M. M., Wade, J. (2004). The Green Anole (Anolis carolinensis): A Reptilian Model for Laboratory Studies of Reproductive Morphology and Behavior. *Institute of Laboratory Animal Resources Journal 45(1)*, 54-64. https://doi.org/10.1093/ilar.45.1.54

Lovern, M. B., McNabb, F. M. A., Jenssen, T. A. (2001). Developmental Effects of Testosterone on Behavior in Male and Female Green Anoles (*Anolis carolinensis*). *Hormones and Behavior 39*, 131-143. https://doi.org/10.1006/hbeh.2000.1637

Lu, H., Qin, L., Lee, K., Wong, W., Chan, K., Leung, K. (2008). Healing Compared Between Bone to Tendon and Cartilage to Tendon in a Partial Inferior Patellectomy Model in Rabbits. *Clinical Journal of Sports Medicine 18(1)*, 62-69. https://doi.org/10.1097/jsm.0b013e31815c24ba

Mackie, E. J., Ahmed, Y. A., Tatarczuch, L., Chen, K. S., Mirams, M. (2008). Endochondral Ossification: How Cartilage is Converted into Bone in the Developing Skeleton. *The International Journal of Biochemistry and Cell Biology 40*, 46-62. https://doi.org/10.1016/j.biocel.2007.06.009

Mandarim-de-Lacerda C. A. (2019). A Brief Introduction to the Evolutionary Anatomy of the Skull and Face in the Genus *Homo*. *Journal of Health and Medical Sciences 5(2)*, 107-111.

Mankin, H. J., Lippiello, L. (1971). The Glycosaminoglycans of Normal and Arthritic Cartilage. *Journal of Clinical Investigation 50(8)*, 1712-1719. https://doi.org/10.1172%2FJCI106660

Maue, W. M., Dickson, D. R. (1971). Cartilages and Ligaments of the Adult Human Larynx. *Arch Otolaryng 94*, 432-439. https://doi.org/10.1001/archotol.1971.00770070678008

Milligan, M. (1946). Trichrome Stain for Formalin-Fixed Tissue. *American Journal of Clinical Pathology 10(6)*, 184-185. https://doi.org/10.1093/ajcp/16.11_ts.184

Miyashita, T., Gess, R.W., Tietjen, K., Coates, M.I. (2021). Non-ammocoete Larvae of Paleozoic Stem Lampreys. *Nature 591*, 408-412. https://www.nature.com/articles/s41586-021-03305-9

Motta, P. J., Hueter, R. E., Tricas, T. C. (1991). An Electromyographic Analysis of the Biting Mechanism of the Lemon Shark, *Negaprion brevirostrus*: Functional and Evolutionary Implications. *Journal of Morphology 210*, 55-69. https://doi.org/10.1002/jmor.1052100106

Nagase, H., Kashiwagi, K. (2003). Aggrecanases and Cartilage Matrix Degradation. *Arthritis Research and Therapy 5(2)*, 94-103. https://doi.org/10.1186/ar630

Natchev, N., Tzankov, N., Vergilov, V., Kummer, Handschuh (2015). Functional Morphology of a Highly Specialized Pivot Joint in the Cranio-Cervical Complex of the Minute Lizard *Ablepharus kitaibelii* in Relation to Feeding Ecology and Behavior. *Contributions to Zoology 84(1)*, 13-23.

Neenan J. M., Ruta M., Clack J. A., and Rayfield E. J. (2014) Feeding Biomechanics in *Acanthostega* and across the Fish-Tetrapod Transition. *Proceedings of the Royal Society B 281*: 20132689. https://doi.org/10.1098/rspb.2013.2689

Nicholson, K. E., Harmon L. J., Losos J. B. (2007). Evolution of *Anolis* Lizard Dewlap Diversity. *PLoS ONE 2*(3), e274. https://doi.org/10.1371/journal.pone.0000274

Nijweide, P. J., Burger, E. H., Feyen, J. H. M. (1986). Cell of Bone: Proliferation, Differentiation, and Hormonal Regulation. *Physiological Reviews 66*(4), 855-886. https://doi.org/10.1152/physrev.1986.66.4.855

Nikolov, S., Fabritus, H., Petrov, M., Friàk, M., Lymperakis, L., Sachs, C., Raabe, D., Neugebauer, J. (2011). Robustness and Optimal use of Design Principles of Arthropod Exoskeletons Studied by ab Initio-Based Multiscale Simulations. *Journal of the Mechanical Behavior of Biomedical Materials 4*, 129-145. http://dx.doi.org/10.1016/j.jmbbm.2010.09.015

Nunn, J. F., Campbell, E. J. M., Peckett, B. W. (1959). Anatomical subdivisions of the volume of respiratory dead space and effect of position of the jaw. *Journal of Applied Physiology 14*(2). 174-176. https://doi.org/10.1152/jappl.1959.14.2.174

Ogston, A., (1875). On Articular Cartilage. *Journal of Anatomy and Physiology 10*, 43-74.

Olivier, D., Van Wassenbergh, S., Parmentier, E., Frédérich, B. (2021). Unprecedented Biting Performance in Herbivorous Fish: How the Complex Biting System of Pomacentridae Circumvents Performance Trade-Offs. *The American Naturalist 197*(5), E156-E172. http://dx.doi.org/10.1086/713498

Ord, T. J., Klomp, D. A., Garcia-Porta, J., Hagman, M. (2015). Repeated Evolution of Exaggerated Dewlaps and Other Throat Morphology in Lizards. *Journal of Evolutionary Biology 28*, 1948-1964. https://doi.org/10.1111/jeb.12709

Orsbon, C. P., Gidmark, N. J., Ross, C. F. (2018). Dynamic Musculoskeletal Functional Morphology: Integrating diceCT and XROMM. *The Anatomical Record 301*, 378-406. https://doi.org/10.1002/ar.23714

Owercowicz T., Farmer C. G., Hicks J. W., Brainerd E. L. (1999). Contribution of Gular Pumping to Lung Ventilation in Monitor Lizards. *Science 284(5420)*, 1661-1663. https://doi.org/10.1126/science.284.5420.1661

Paget, J. (1855). Account of a Growth of Cartilage in a Testicle and its Lymphatics, and in Other Parts. *Medico-Chirurgical Transactions 38*, 247-260.

Peabody J. E. (1897). The Ampullae of Lorenzini of the Selachii. *Zoological Bulletin 1(4)*, 163-178. https://doi.org/10.2307/1535427

Pierce, S. E., Clack, J. A., Hutchinson, J. R. (2012). Three-Dimensional Limb Joint Mobility in the Early Tetrapod Ichthyostega. *Nature 486*, 523-527. https://doi.org/10.1038/nature11124

Puchtler, H., Meloan, S. N., Terry, M. S. (1969). The History and Mechanism of Alizarin and Alizarin Red S Stains for Calcium. *The Journal of Histochemistry and Cytochemistry 17(2)*, 110-124. https://doi.org/10.1177/17.2.110

Reisz, R. R. (1997). The Origin and Early Evolutionary History of Amniotes. *TREE 12*(6), 218-222. https://doi.org/10.1016/S0169-5347(97)01060-4

Robson, P., Wright, G. M., Youson, J. H., Keeley, F. W. (1997). A Family of Non-Collagen-Based Cartilages in the Skeleton of the Sea Lamprey *Petromyzon marinus*. *Compositional and Biochemical Physiology 118B(1)*, 71-78. https://doi.org/10.1016/S0305-0491(97)00026-6

Rogers, B. T., Peterson, M. D., Kaufman T.C. (2002). The Development and Evolution of Insect Mouthparts as Revealed by the Expression Patterns of Gnathocephalic Genes. *Evolution and Development 4*(2), 96-110. https://doi.org/10.1046/j.1525142x.2002.01065.x

Roughley, P. J. (2006). The Structure and Function of Cartilage Proteoglycans. *European Cells and Materials 12*, 92-101. https://doi.org/10.22203/ecm.v012a11

Rowe, A. J., Snively, E. (2022). Biomechanics of Juvenile Tyrannosaurid Mandibles and their Implications for Bite Force: Evolutionary Biology. *The Anatomical Record 305*, 373-392. https://doi.org/10.1002/ar.24602

Rufai, A., Benjamin, M., Ralphs, J. R. (1995). The Development of Fibrocartilage in the Rat Intervertebral Disc. *Anatomical Embryology 192*, 53-62. https://doi.org/10.1007/bf00186991

Ruxton, G. D., Houston, D. C. (2004). Obligate Vertebrate Scavenger Must Be Large Soaring Fliers. *Journal of Theoretical Biology 228*, 431-436. https://doi.org/10.1016/j.jtbi.2004.02.005

Scott J. E., Quintarelli, G., Dellovo, M. C. (1964). The Chemical and Histochemical Properties of Alcian Blue I. the Mechanism of Alcian Blue Staining. *Histochemie 4*, 73-85. https://doi.org/10.1007/bf00306149

Scott S. H. and Winter D. A. (1991). Talocrural and Talocalcaneal Joint Kinematics and Kinetics During the Stance Phase of Walking. *Journal of Biomechanics 24(8)*, 743-752. https://doi.org/10.1016/0021-9290(91)90338-n

Schilttuizen, M., van Til, A., Salverda, Liew, T., James, S. S., bin Elahan, B., Vermeulen, J. J. (2006). Microgeographic Evolution of Snail Shell Shape and Predator Behavior. *Evolution 60(9)*, 1851-1858. https://doi.org/10.1111/j.00143820.2006.tb00528.x

Schubert, M., Escriva H., Xavier-Neto, J., Laudet V. (2006). Amphioxus and Tunicates as Evolutionary Model Systems. *TRENDS in Ecology and Evolution 21*(5), 269-277. https://doi.org/10.1016/j.tree.2006.01.009

Seidel. R., Jayasankar, A. K., Dean M. N. (2021). The Multiscale Architecture of Tessellated Cartilage and its Relation to Function. *Journal of Fish Biology 98*, 942-955. https://doi.org/10.1111/jfb.14444

Shimeld, S. M., Donoghue, P.C.J. (2012). Evolutionary Crossroads in Developmental Biology: Cyclostomes (Lamprey and Hagfish). *Development 139*(12), 2091-2099. https://doi.org/10.1242/dev.074716

Shimizu, Y., Kanetaka, H., Kim, Y, Okayama, K., Kano, M., Kikuchi, M. (2005). Age-Related Morphological Changes in the Human Hyoid Bone. *Cells Tissues Organs 180*, 185-192. https://doi.org/10.1159/000088247

Shu, D. G., Morris, S. C., Han, J., Zhang, Z. F., Liu, J. N. (2002). Ancestral echinoderms from the Chengjiang deposits of China. *Nature 430*, 422-428. https://doi.org/10.1038/nature02648

Signor, P. W., Brett, C. E. (1984). The Mid-Paleozoic Precursor to the Mesozoic Marine Revolution. *Paleobiology. 10*(2), 229-245.

Singer, R. A. (2014) Are Dehydrated Specimens a Lost Cause? A Case Study to Reclaim Dehydrated Fluid Preserved Specimens. *Collection Forum 28(1-2)*, 16-20. http://dx.doi.org/10.14351/0831-4985-28.1.16

Stephenson, A., Adams, J. W., Vaccarezza M. (2017). The Vertebrate Heart: An Evolutionary Perspective. *Journal of Anatomy 231*, 787-797. https://doi.org/10.1111/joa.12687

Tassia, M. G., Cannon, J. T., Konikoff, C. E., Shenkar, N., Halanych, Swalla B. J. (2016). The Global Diversity of Hemichordata. *PLoS ONE 11*(10). E0162564. https://doi.org/10.1371%2Fjournal.pone.0162564

Tapanila, L., Pruitt, J., Pradel, A., Wilga, C. D., Ramsay, J. B., Schlader, R., Didier, D. A. (2013). Jaws for a Spiral-Tooth Whorl: CT Images Reveal Novel Adaptation and Phylogeny in Fossil Helicoprion. *Biological Letters 9*, 20130057. https://doi.org/10.1098/rsbl.2013.0057

Thompson, Z., Miclau, T., Hu, D., Helms, J. A. (2002). A Model for Intramembranous Ossification During Fracture Healing. *Journal of Orthopaedic Research 20*, 1091-1098. https://doi.org/10.1016/s0736-0266(02)00017-7

Tsai, W., Chen, W., Chien, H., Kuo, W., Wang, M. (2011). Poly(dopamine) Coating of Scaffolds for Articular Cartilage Tissue Engineering. *Acta Biomaterialia 7*, 4187-4194. https://doi.org/10.1016/j.actbio.2011.07.024

Tsuchiya, H., Ueda, Y., Morishita, H., Nonomura, A., Kawashima, A., Fellinger, E. J., Tomita, K. (1993). Borderline Chondrosarcoma of Long and Flat Bones. *Journal of Cancer Research and Clinical Oncology 119*, 363-368. https://doi.org/10.1007/bf01208847

Uyeda, J. C., Zenil-Ferguson, R., Pennell, M. W. (2018). Rethinking Phylogenetic Comparative Methods. *Systematic Biology 67*(6), 1091-1109. https://doi.org/10.1093/sysbio/syy031

Vanhooydonck, B., Herrel, A., Meyers, J. J., Irschick, D. J. (2009). What Determines Dewlap Diversity in *Anolis* Lizards? An Among Island Comparison. *Journal of Evolutionary Biology 22*, 293-305. https://doi.org/10.1111/j.14209101.2008.01643.x

Vanhooydonck, B., Herrel, A. Y., Van Damme, R., Irschick, D. J. (2005). Does Dewlap Size Predict Male Bite Performance in Jamaican *Anolis* Lizards. *Functional Ecology 19*, 38-42. https://doi.org/10.1093%2Fcz%2Fzoy041

Vanhooydonck, B., Herrel, A. Y., Van Damme, R., Irschick, D. J. (2005). Does Dewlap Size Predict Male Bite Performance in Jamaican *Anolis* Lizards. *Functional Ecology 19*, 38-42. https://doi.org/10.1111/j.0269-8463.2005.00940.x

Van Valkenburgh B. (2007). Déja Vu: The Evolution of Feeding Morphologies in the Carnivora. *Integrative and Comparative Biology 47*(1), 147-163. https://doi.org/10.1093/icb/icm016

Vejlens, L. (1971). Glycosaminoglycans of Human Bone Tissue. *Calcified Tissue Research 7*, 175-190.

Von Geldern, C. E. (1919). Mechanism in the Production of the Throat-Fan in the Chameleon, *Anolis carolinensis*. *Proc. Calif. Acad. Sci., 9*: 313-329.

Wainwright, P. C., Alfaro, M. E., Bolnick, D. I., Hulsey, C. D. (2005). Many-to-one mapping of form to function: a general principle in organismal biology? *Integrative and Comparative Biology 45*, 256-262. https://doi.org/10.1093/icb/45.2.256

Walters, M., Crew, M., Fyfe, G. (2019). Bone Surface Micro-Topography at Craniofacial Entheses: Insights on Osteogenic Adaptation at Muscle Insertions. *The Anatomical Record 302*, 2140-2155. https://doi.org/10.1002/ar.24215

Wang, X., Bank, R. A., TeKoppele, J. M., Agrawal, C. M. (2001). The Role of Collagen in Determining Bone Mechanical Properties. *Journal of Orthopaedic Research 19*, 1021-1026. https://doi.org/10.1016/s0736-0266(01)00047-x

Watkins, J. (2014). Biomechanics of Musculoskeletal Adaptation. *Comprehensive Biomedical Physics 10*, 1-37.

Westneat M. W. (2004). Evolution of Levers and Linkages in the Feeding Mechanisms of Fishes. *Integrative and Comparative Biology 44*, 378-389. https://doi.org/10.1093/icb/44.5.378

Williams, H. (2001). Choreography of song. Dance, and beak movements in the zebra finch (*Taeniopygia guttata*). *The Journal of Experimental Biology 204*, 3497-3506.

Williams, T. M., Carroll, S. B. (2009). Genetic and molecular insights in the development and evolution of sexual dimorphism. *Nature Reviews 10*, 797-804. https://doi.org/10.1242/jeb.204.20.3497

Williams, T. W. (1941). Alizarin Red S and Toluidine Blue for Differentiating Adult or Embryonic Bone and Cartilage. *Stain Technology 16(1)*, 23-25. https://doi.org/10.3109/10520294109106191

Witherington, C. W. (1925). The Histogenesis of Bone. *Journal of Anatomy 59(2)*, 136-154.

Wolfgang, M., Ruf, I. (2016). Evolution of the Mammalian Middle Ear: A Historical Review. *Journal of Anatomy 228*, 270-283. https://doi.org/10.1111%2Fjoa.12379

Xian-guang, H., Aldridge, R. J., Siveter, D. J., Siveter, D. J., Xiang-hong, F. (2002). New Evidence on the Anatomy and Phylogeny of the Earliest Vertebrates. *Proceedings of the Royal Society of London B 269*, 1865-1869 https://doi.org/10.1098%2Frspb.2002.2104.

Yakut, Y., Tuncer, A. (2020). Architecture of Human Joints and Their Movement. *Normal and Pathological Conditions*, 47-57.

Yotsuyanagi, T., Yamauchi, M., Yamashita, K., Sugai, A., Gonda, A., Kitada, A., Saito, T., Urushidate. (2015). Abnormality of Auricular Muscles in Congenital Auricular Deformities. *Reconstructive 136*(1), 78e-88e. https://doi.org/10.1097/prs.0000000000001383

Zhigkh, L., Vangysel, E., Nonclerqc, D., Legran, A., Blairon, B., Berri, C., Bordeau, T., Rémy, C., Burtéa, C., Montuelle, S. J., Bels, V. (2014). Morphology and Fibre-Type Distribution in the Tongue of the *Pogona vitticeps* lizard (Iguania, Agamidae). *Journal of Anatomy 225*, 377-389. https://doi.org/10.1111%2Fjoa.12224

VITA

Jacob William George

Candidate for the Degree of

Master of Science

Thesis: A REANALYSIS OF THE ANOLE DEWLAP AT THE OSTEOLOGICAL, HISTOLOGICAL, AND MYOLOGICAL LEVELS

Major Field: Biomedical Sciences

Biographical:

Education:

Completed the requirements for the Master of Science in Biomedical Sciences at Oklahoma State University, Stillwater, Oklahoma in July, 2022.

Completed the requirements for the Bachelor of Science in Biology at West Virginia University, Clarksburg, West Virginia in 2020.

Experience:

2021	Summer Session Research Technician Oklahoma State University Center for Health Sciences, Tulsa, OK
2020-2022	Graduate Research Assistant Oklahoma State University Center for Health Sciences, Tulsa, OK
2019	Undergraduate Lab Assistant West Virginia University, Morgantown, WV

Presentations:

2022 **George, J.**, Browne, I., Gignac, P., Claxton, A., O'Brien, H. "Designing 3D printed braces for imaging the Carolina anole (*Anolis carolinensis*) dewlap musculature using diceCT" *Society for Integrative and Comparative Biology 2022*.